INTRODUCING A NEUTRON DETECTOR MODEL INTO THE OSCAR 3 CALCULATIONAL CODE SYSTEM AND VALIDATION WITH KOEBERG REACTOR CALCULATIONS

by

Mzubanzi Bismark Tyobeka

A mini-dissertation presented to the Faculty of Agriculture, Science and Technology

of the

UNIVERSITY OF NORTH-WEST

for the partial fulfillment of the degree of

MAGISTER SCIENTIAE

(Applied Radiation Science and Technology)

Promoter:

Mr. F. Reitsma

Radiation and Reactor Theory

South African Nuclear Energy Corporation

Co-Promoter:

Dr. W. Joubert

Radiation and Reactor Theory

South African Nuclear Energy Corporation

INTRODUCING A NEUTRON DETECTOR MODEL INTO THE OSCAR 3 CALCULATIONAL CODE SYSTEM AND VALIDATION WITH KOEBERG REACTOR CALCULATIONS

by

Mzubanzi Bismark Tyobeka

A mini-dissertation presented to the Faculty of Agriculture, Science and Technology

of the

UNIVERSITY OF NORTH-WEST

for the partial fulfillment of the degree of

MAGISTER SCIENTIAE

(Applied Radiation Science and Technology)

Promoter:

Mr. F. Reitsma

Radiation and Reactor Theory

South African Nuclear Energy Corporation

Co-Promoter:

Dr. W. Joubert

Radiation and Reactor Theory

South African Nuclear Energy Corporation

INTRODUCING A NEUTRON DETECTOR MODEL INTO THE OSCAR 3 CALCULATIONAL CODE SYSTEM AND VALIDATION WITH KOEBERG REACTOR CALCULATIONS

Mzubanzi Bismark Tyobeka

Mmabatho

2001

ABSTRACT

The objective of this research is to develop accurate and efficient computational methods of predicting neutron detector responses by introducing a neutron detector model into the OSCAR-3 code system. The importance of the nodal and homogenization schemes in reactor analysis is demonstrated by using a nodal diffusion code, ***MGRAC***, to perform core calculations for the Koeberg reactor so as to validate the detector model that is being developed in this study. The measure of determining the detector response used in this study is referred to as the detector constant and is taken to be the ^{235}U microscopic fission cross-section. Both the one group and two group detector constant methods are investigated and tested in developing a suitable detector model for this code in this study.

Sensitivity studies are carried out to evaluate the sensitivity of the detector constant to changes in core parameters such as the moderator temperature, fuel temperature, boron concentration, assembly type and also to investigate the behaviour of the detector constant as a function of burnup.

Two methodologies are used to calculate the detector responses in this study viz., the average flux method (which takes into account the average flux over the whole assembly) and the flux reconstruction method (which takes into account the flux at the centre of the assembly where the detector is inserted). The results obtained for both these methods (from the ***MGRAC*** code) are compared to the plant detector values and their accuracy is determined by calculating the maximum absolute % error and the root mean square (rms.) % error for each method. These calculations are performed for the two-group detector constant. The observation is that both the average and reconstructed flux models yield fairly accurate results, but owing to its affordability and less time-consuming nature, the average flux model is recommended for implementation into the OSCAR-3 code and for use in the production runs of the Koeberg Nuclear Power Station.

ACKNOWLEDGEMENTS

The successful completion of this work is attributed to the following people, whose tireless efforts are highly appreciated:

1. My promoter Mr. Frederik Reitsma, who, despite his very tight schedule has always been there to provide the necessary supervision and guidance that led to the ultimate completion of this work.

2. The staff of the Radiation and Reactor Theory Group of NECSA in general, and in particular, Dr. Wessel Joubert whose contribution in familiarizing me with the computer code HEADE for use in this study, Ms. Diana Naidoo for her assistance with MGRAC and most of all Mrs. Hantie Labuschagne who made sure that this manuscript is well typed, consistent and well arranged.

3. My sponsors, ESKOM Enterprises, who made sure that I continue to receive financial support and living allowances during the daunting task of carrying out this research.

4. The staff at the Center for Applied Radiation Science and Technology in my University for making sure that all the logistical support was given during the pursuance of this work.

5. My family and in particular, my mother who despite all the sufferings she had to endure because of having to fend for me, has never given up hope that one day this work will be completed successfully.

6. Above all, to the Almighty God who defended and protected me under trying and incredible circumstances during all my years of schooling.

TABLE OF CONTENTS

LIST OF TABLES

LIST OF FIGURES

APPENDICES

NOMENCLATURE

1-D	one-dimensional
2-D	two-dimensional
AEC	atomic energy corporation of South Africa
BPs	burnable poisons
BWRs	boiling water reactors
ENDF	evaluated nuclear data files
FVW	flux volume weighted
HEADE	heterogeneous assembly depletion code
MOX	mixed oxide
MW/te	megawatt thermal
MW/e	megawatt electrical
MGRAC	multigroup assembly depletion code
NECSA	nuclear energy corporation of South Africa
OSCAR-3	overall system for the calculation of reactors - version 3
PWR	pressurized water reactor
SCIENCE	Framatome core calculational code system (used at Koeberg)

CHAPTER 1 INTRODUCTION

1.1 Overview

Modern day reactor core analysis requires an accurate determination of the behaviour of the neutron population as distributed in space, direction and energy (Duderstadt et al, 1976). Entities such as the neutron densities, flux, core power distribution, control rod worth, shutdown margins, isotopic depletion rates and neutron interaction and reaction rates should be known at any stage throughout the reactor cycle. They are essential for, amongst others, licensing, fuel performance, thermal hydraulics and most importantly, core- follow safety calculations. The safety and economics of nuclear power plants across the globe rely heavily on these computational analyses with the consequent incentive to develop codes and methods to accurately predict the neutron distribution. Another alternative would also be to improve the existing codes that are being used for reactor core analysis. Even today, modern fuel designs, with their associated increase in complexities in terms of their geometry and material compositions give yet another daunting task to reactor physicists and new challenges to theoretical support resources. The use of MOX (mixed oxide) assemblies, Gadolinium poisons in shim control, axial blanket regions and differential enrichments are just a few of these modern trends.

The behaviour of a nuclear reactor is governed by the distribution in space, energy and time of the neutrons in the system, and one of the central problems of reactor theory is to predict or devise means to determine this distribution. In principle, this can be done by solving the neutron transport equation, often called the Boltzmann equation because of its similarity to the expression obtained by L. Boltzmann in connection with the kinetic theory of gasses (Bell et al, 1970]. Inserting a complete set of appropriate cross sections, which represent the neutron interaction probabilities, into the transport equation, together with the geometrical arrangement of the materials in the system, could solve the neutron

distribution problem. Numerical solutions could then be obtained by suitable computational procedures, e.g. Monte Carlo methods. In practice however, this proves not to be practical. Firstly, the cross sections and their variation with neutron energy are very complicated and secondly, the geometric arrangement of the materials in the reactor is so complex that the transport equation cannot be solved in reasonable time even with today's fast computers. The approximation to the transport equation of importance in this work, is the group diffusion theory model, especially in core-follow calculations. There are many instances in nuclear reactor analysis in which one requires a full-three-dimensional calculation of the neutron flux, for example, in core fuel depletion or control-rod movement studies. In such instances, it is desired that we must have a scheme for determining the three-dimensional core flux distribution that avoids the large storage and execution time requirements of a direct finite difference treatment of the diffusion equation. Such a scheme is provided by the so-called nodal methods, which are employed in this work when core follow calculations are performed. The general idea is to decompose the reactor core into relatively large sub-regions or nodes in which the material composition and flux are assumed uniform (Duderstadt et al, 1976) or at least treated in an average sense. Modern or the so-called advanced nodal methods are accurate and capable of predicting assembly-averaged powers within 2% (Sesonske, 1981).

1.2 Introduction to Core Monitoring Instrumentation and Detector Modelling

Evaluation of the actual accuracy of computed power distribution in the reactor can only be determined by comparisons with actual plant data such as the measured in-core detector response. In-core instrumentation has generallly consisted of fluence measuring devices plus thermocouples placed at centres of the exit nozzles of a number of fuel assemblies. Mixing vanes are often placed at fuel assembly outlets to assure that thermocouple

measurements reflect true bundle–average outlet temperatures. In-core flux measuring devices have taken a variety of forms. They have included:

1. *Flux wires*: Flexible wires inserted into the core at a number of radial positions and irradiated for a pre-set time. Wires are then removed from the core and counted. Wire activation is proportional to flux and, hence, axial flux variation is determined by axial variation in wire activity (Tong et al, 1979).

2. *Movable in-core detectors*: Detectors connected to flexible cables that can move detectors axially in fixed radial positions. By making a traverse of the core, axial variation in flux at a given *x-y* location is determined. Detectors can be kept out of the core when not in use and, hence, radiation damage is limited.

3. *Fixed in-core detectors*: At given *x-y* locations, several fixed detectors are located at a series of axial positions. These detectors provide a continuous picture of core-flux distribution.

While there are many different types of in-core detectors (e.g. fission chambers, rhodium wires, gamma detectors, etc.) as described above, the most widespread is moveable ^{235}U fission chambers (the structure of which is described in the next section). Such detectors are used periodically to assess the in-core power distribution. Strictly speaking, the detector system is measuring the relative reaction rate of ^{235}U in the central instrument thimble of each instrumented fuel assembly. The accurate modelling of the detector is therefore an essential part in core monitoring analysis. This work focuses on developing a detector model for the Koeberg PWRs and evaluating the efficiency of that model by comparing the results obtained when using a calculation code that incorporates this detector model with the results or measurements obtained from the actual plant data. Reference is frequently made to “measured” assembly power distributions, however, such

inferred power distributions actually rely on computed reaction rate-to-power conversion factors, which are obtained from a calculational model or are taken from specifications of the suppliers. This introduces uncertainties into both the measured assembly power and calculated power since the same set of conversion factors (or cross sections) may be used. In order to avoid these ambiguities, it is proposed that it would be more appropriate to compare computed detector reaction rates to the measured reaction rate, which is directly proportional to the measured volt readings captured by the plant computer. This is consequently also the approach followed in the rest of this work.

1.3 PWR Detector Positions

In order to accurately give a precise interpretation of the status of a core, there is a need to simulate ways of detecting the distribution of neutrons in the core of a reactor. Sub-miniature fission chambers are used in most PWRs as neutron detecting devices. These sub-miniature fission chambers contain about 200 μg of fissile material (^{235}U in this work), with a tight 'feed-through' between the fission chamber body and the coaxial wire (see ***Figure 1-1***). Such a detector is expected to have an efficiency of about 10^{-18} A/n.cm^{-2}s^{-1} and to be directly sensitive to neutron fluence (Guyard et.al, 1997).

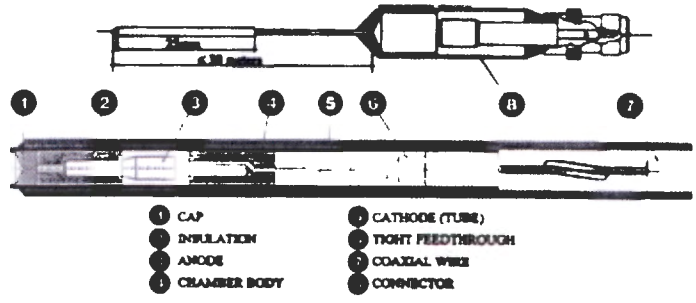

Figure 1-1: State-of-the-Art Fission Chamber

The Koeberg reactor is a Pressurised Water Reactor (PWR) that accounts for approximately 8% of the production of electricity in South Africa. Being the only South African power reactor, Koeberg is situated on the West Coast, about 25 km from Cape Town. It has two reactor units each with 920 MW power output, a 17 X 17 Westinghouse design reactor built by Framatome in 1976 and started operation on 04 April 1984.

The core of this reactor comprises an array of 157 fuel assemblies (***Figure 1-2***), which are identical in design but different in fuel enrichment. A fuel assembly consists of 264 fuel rods joined in a 17x17 square array. The fuel rod consist of slightly enriched uranium dioxide pellets contained in sealed Zircaloy-4 tubing, 4 m long and 10 mm in diameter. ***Figure 1-2*** shows the arrangement of assemblies in such a 17 x 17 Westinghouse design.

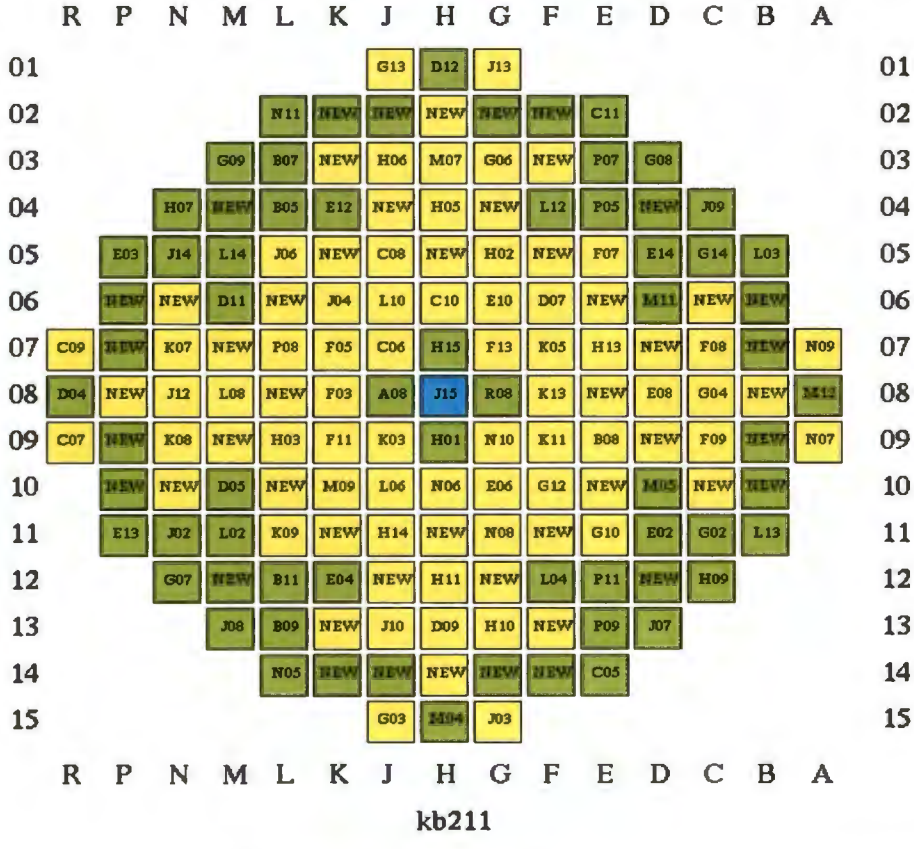

Figure 1-2: The Koeberg Core: A 17 x 17 Westinghouse assembly design

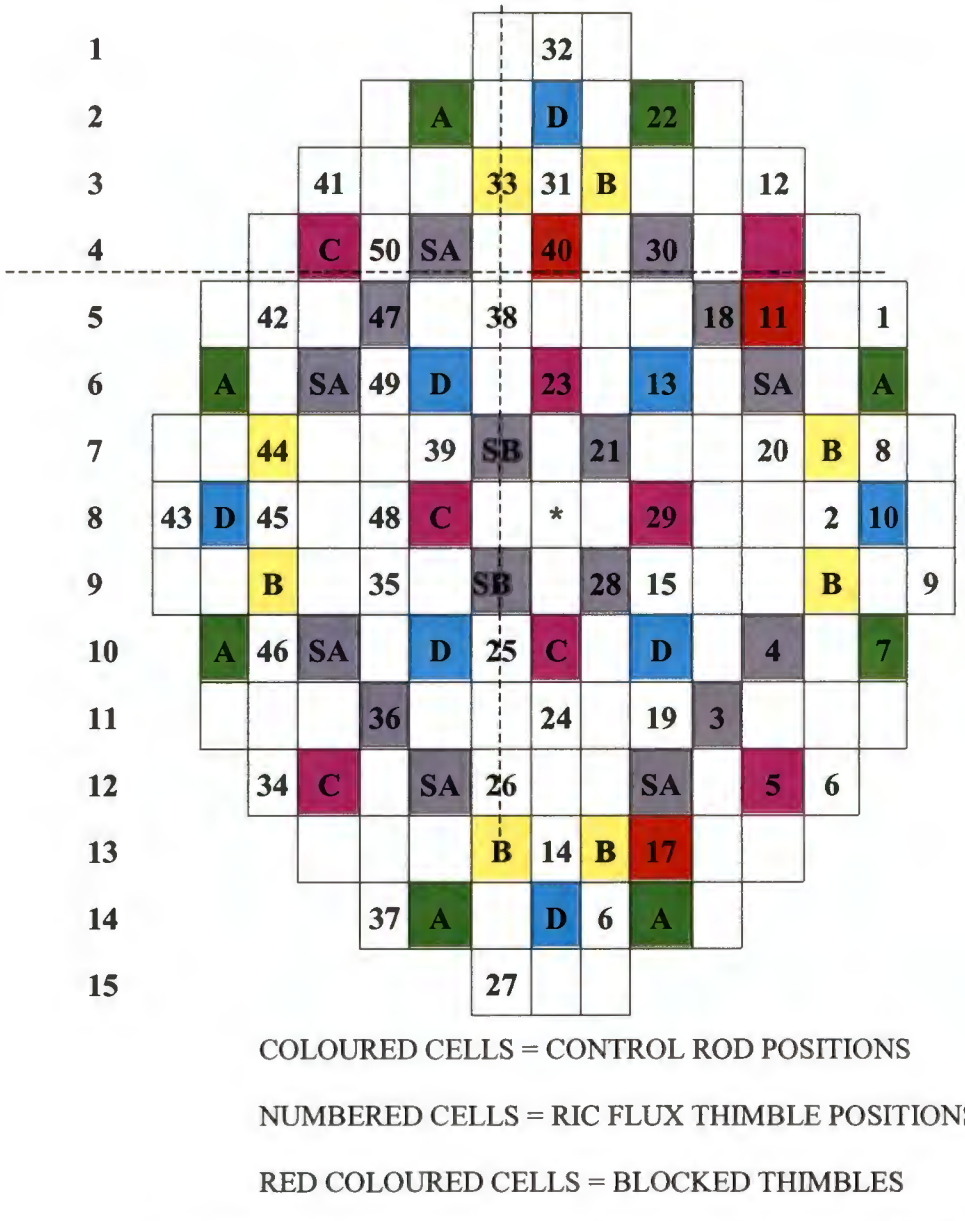

Figure 1-3: Instrumented Fuel Assemblies in the Koeberg Unit 2 Reactor

Figure 1-3 shows the locations of the instrumented fuel assemblies in the Koeberg reactor for unit 2. In these assemblies, detectors are moved in thimbles inserted in guide tubes (usually centrally located). Signals generated by these mobile detectors are proportional to the activity produced by neutrons in ^{235}U of the detector i.e. there exist a linear relationship between fission rate and power. Together, all the signals obtained from the detector 'd' as

it moves through channel 'K' during pass 'p' are known as a trace. At each pass, detectors are inserted into the core through the vessel bottom head and are routed to the top of the active core. Detector motion is evaluated in a number of encoder steps (1 encoder step is about 1 mm). The acquisition of measurements is performed during the down-core phase. When 8 encoder steps have been counted, a signal is sent to the computer, which digitises the signal supplied by the detector. One basic measurement therefore covers about 8 mm of the core.

Two examples of traces in a fresh fuel assembly and a spent fuel assembly are given in the upper graphs of ***Figure 1-4*** and ***Figure 1-5*** respectively. As may be seen from the figures, the trace for a fresh assembly appears to be a smooth parabolic curve (except for the dips caused by flux depression) but for the depleted assembly, the shape is flatter in the middle of the core because this is where the assembly has higher burnup.

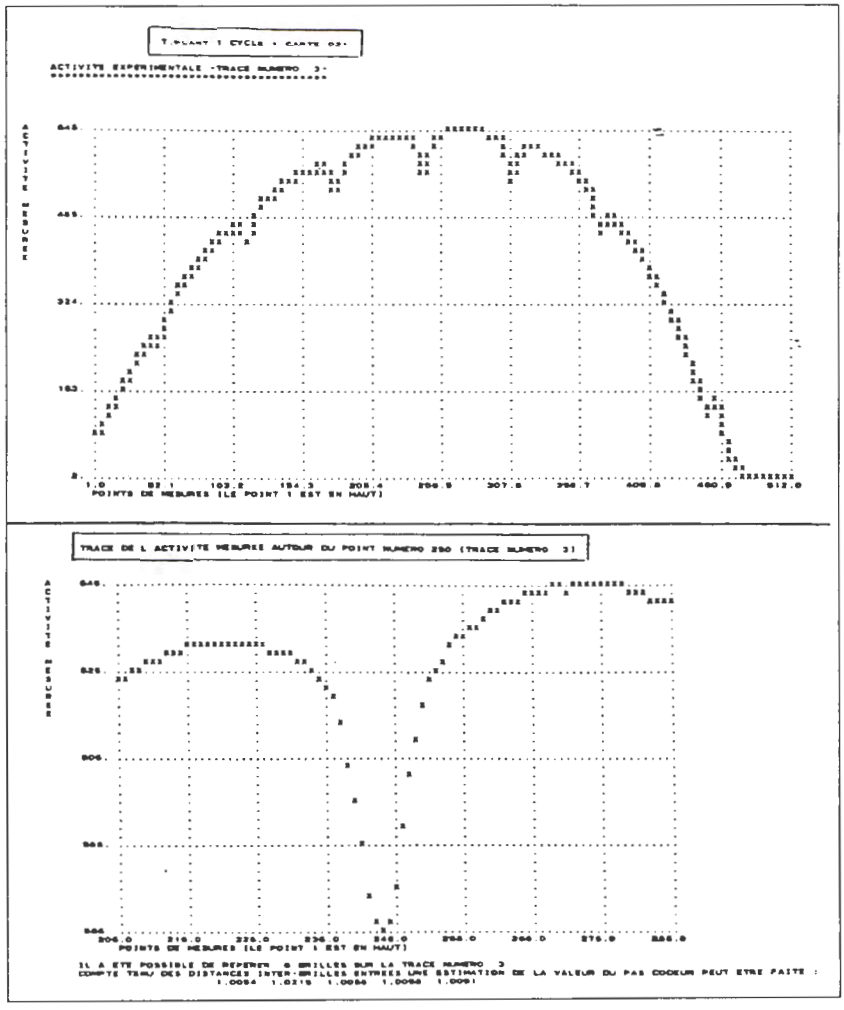

Figure 1-4: Typical trace for a fresh assembly

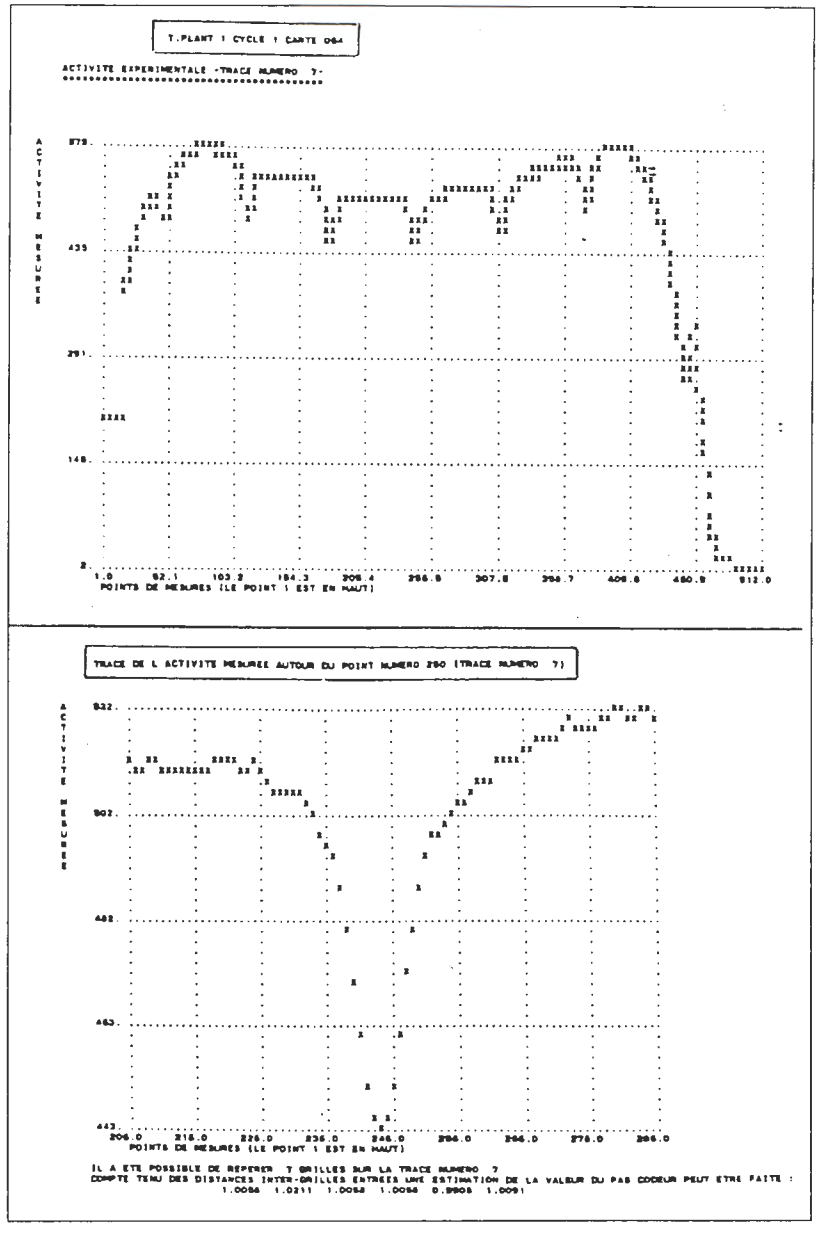

Figure 1-5: Typical trace for a depleted assembly

Some detail of the "dips" in the measurements is illustrated in the lower graphs of ***Figure 1-4*** and ***Figure 1-5***, which are enlargements of the measurements taken in the axial region around a spacer grid. These spacer grids are 37 mm high and are made of inconel and are there to hold the assembly structure together. The resultant flux depression can be very pronounced and is normally used to solve the problem of axial positioning and the corresponding adjustment of traces. This flux depression around the spacer grid is caused by two reasons. Firstly, inconel has a larger absorption cross section than that of other

structural materials used in the assembly. Secondly, the grids displace water at these positions, and therefore the slowing-down effect is reduced and the spectrum becomes harder resulting in a lower fission rate and detector measurement.

1.4 Justification for this Work and its Objectives

In the preceding section, a depiction of the actual physical situation of what this work will attempt to simulate/model and fit into a calculational code system, has been given. It must also be noted that due to different assembly types in the Koeberg core, several detector environments have to be simulated for each of those assembly types. The interesting feature of these envisaged models is how they respond to different changes in the localised core (or assembly) parameters e.g. fuel temperature, density, moderator temperatures, etc. - the so-called sensitivity studies.

This dissertation is concerned with investigating a detector model, which must be built into the OSCAR-3 calculational code system used to perform core-follow calculations for the Koeberg reactor. This exercise will also validate this computer code, which, without such a detector model, could not be compared with Koeberg in-core detector measurements before. To make this task possible, many theoretical arguments must be taken into consideration. Reaction rates calculated from nodal diffusion methods will be used to determine the detector response as some of the above-mentioned core parameters are varied. This work will contribute to a better understanding of how detectors respond to changes in the core conditions. The measure of the detector response to be used in this study is the fission cross section of ^{235}U and will herein be referred to as the detector constant.

The success of this work will give developers of the OSCAR-3 code a tool to verify their Koeberg calculations and thus also provide the Koeberg engineers with an alternative and

more flexible tool to perform the safety and reload calculations in a more cost-effective way. This is the case because when this envisaged detector model proves to be accurate enough, and it can then be built into the OSCAR 3 code and yield the above-mentioned incentive.

1.5 Layout of this Dissertation

In the present chapter, the use of the neutron diffusion and transport theory in trying to address the problem of reactor core analysis is explained. Also, a brief synopsis on the fundamental importance of using the nodal diffusion method in core analysis is given, with special emphasis on the interrelationship of both the transport and diffusion theory in tackling problems of reactor core analysis, notably, in developing our envisaged detector model. The physical description of the detectors as they are used in a reactor and how measurements of activity are taken and processed has also been accounted for in this chapter. Finally, the objectives of this work and its economic and scientific value are explained.

In ***Chapter 2***, a detailed theoretical basis for the development of a neutron detector model is given, with attention given to the concepts of assembly homogenization, group collapsing and the use of the nodal average fluxes or using reconstructed fluxes at the detector position for determining the reaction rate in the detector regions. The principles of a two-group diffusion method and flux reconstruction method are consequently also further explored. A brief description of the nodal diffusion code, MGRAC and a transport code, HEADE, is also given.

Chapter 3 deals with the assembly description, the calculation methodology and the results obtained from using HEADE in preparing our cross section library for Koeberg, and

these are interpreted and their actual implications on the outcome of the final detector model are discussed.

Chapter 4 deals with the actual methodology of how core calculations were performed and how the model was tested and incorporated into the code. The results of the calculations are presented and described at length. In ***Chapter 5***, the outcome of the calculations and how they compare to plant data and to other validated codes' results are laid out and discussed. Conclusions drawn from these outcomes and recommendations for future research are also presented in this chapter.

1.6 Notation

The standard mathematical notation used in reactor physics is used throughout this dissertation and in particular, the following quantities are also often used:

- σ Microscopic cross section of a material (barns)
- ϕ Neutron flux density distribution ($n.cm^{-2}.s^{-1}$)
- Σ Macroscopic cross section of a material (cm^{-1})
- σ_f Microscopic fission cross section (barns)
- J Net neutron current density ($n.cm^{-2}.s^{-1}$)
- φ Group flux distribution ($n.\ cm^{-2}.s^{-1}$)

CHAPTER 2 THE DETECTOR MODEL: A THEORETICAL BASIS

2.1 Introduction and Statement of the Problem

In PWR core neutronic calculations, factors like the axial movement of control rods, modern assembly design and axial variation in moderator density necessitates 3-dimensional core analyses. The only practical methods with true three-dimensional capabilities are the nodal diffusion methods. In nodal diffusion calculations, the assemblies are modelled as homogenized regions. In the homogenization process the detailed heterogeneous information, such as the pin fluxes and reaction rates, are lost since it is not possible to define homogenized (or averaged) cross sections that would retain this information (Muller, 1994). The dehomogenization methods attempt to do just that by reconstructing the detailed heterogeneous information. The homogenization process rather attempts to conserve average or integrated quantities. In this respect the node averaged flux, surface currents and reactor eigen-values are generally assumed to be the most important quantities. Provided that accurate homogenized parameters can be determined, modern nodal methods are capable of accurately determining these averaged reactor parameters.

Traditionally, most homogenization schemes only focus on preserving the reaction rates (Smith, 1986). Detailed two-dimensional transport assembly calculations are performed in order to include all transport effects and to take all heterogeneities into account. The assembly calculation is normally performed with zero net current boundary conditions. The assembly heterogeneous flux is the actual (absolute) heterogeneous flux while the average homogenized flux is just the average heterogeneous assembly flux. The homogenized diffusion parameters and assembly-homogenized cross-sections are then calculated by flux volume weighting. This is the methodology used in this study.

Having briefly highlighted the importance of using the above methods in core analysis, it is essential at this stage to mention that the main problem that this work will attempt to address is whether to : (a) use the averaged flux of the node to calculate detector reaction rates, or (b) use the flux reconstruction methods to get the flux in the exact detector position to calculate the detector reaction rates. Mathematically, this problem can be shown as follows:

(a) $\mathrm{Re}action\,Rate = \phi_{av} \bullet \sigma_f$

OR

(b) $\mathrm{Re}action\,Rate = \phi_{\mathrm{det}} \bullet \sigma_f$

Note that $\phi_{\mathrm{det}} = \phi_{\mathrm{det}}^{het} = \quad \phi^{\mathrm{hom}} \bullet F$ and $F = \dfrac{\phi_{\mathrm{det}}^{\ het}}{\phi^{het}_{\ av}}$ (from assembly calculations) ϕ_{av} and ϕ_{det} are the nodal averaged homogenised flux and flux at the detector position, respectively. $\phi^{hom}_{av} = \phi^{het}_{av}$ only in assembly calculations with white boundary conditions.

In short, the method mentioned in option (b) will in this work be referred to as the flux reconstruction model and the one in option (a) as the nodal average model. It is important to understand these methods in-depth because they are the guiding principles upon which our detector model will be based. The sections that follow will deal with an in-depth discussion of these principles.

2.2 Nodal Methods

In many reactor calculations, detailed pin-cell powers are not sought directly, and less detailed quantities such as k_{eff} and average assembly powers are of primary importance. In this case, the elaborate calculation of detailed power distributions (merely to obtain their

averages) is wasteful, and nodal methods, which regard the averaged quantities directly as unknowns, become attractive (Khalil, 1989).

In the application of nodal methods, the core is first partitioned into relatively large volumes called nodes which are typically the size of a fuel assembly in the radial (x-y) plane and approximately 20 cm in height. A rigorous statement of neutron balance is then derived for each node by integration of the transport equation over all directions, over each energy group, and over the volume of each node. If the nodal parameters (flux and volume weighted group cross sections) are assumed to be known for each node, the unknowns of the nodal balance equation are (for each group) the node-volume averaged flux and the node-surface averaged net currents. The solution of this equation thus requires a specification of additional relationships between the face-average currents and the node-average fluxes (Duderstadt et al 1976).

2.2.1 Early Nodal Methods

Amongst the earliest nodal models (and some of the advanced models) are those that adopt an extremely simple approach to core neutronics. Typically, a one-group neutron balance is written for each node in which it is customary to assume that the node is coupled only to its nearest neighbours. The inter-node currents are related to the node-average fluxes using transport kernels that are usually synthesized in simple ways using nodal values of k_∞ (the infinite multiplication). An improved class of nodal codes, based on $1^1/_2$-group methods, is also routinely used for reactor lifetime calculations. Although such codes have some attractive features (e.g. treatment of larger cores, improved thermal-hydraulics models, more elaborate fits of the depletion-dependent nodal parameters), they are still limited by the need for adjustment of input parameters to improve agreement with more rigorous methods (Khalil, 1983.)

Despite the limitations of most of the 1-group and $1^1/_2$-group nodal methods, their use also offers a number of advantages. For example, by adopting simple approaches to the neutronic calculations, computer storage requirements are reduced, and the complicated sets of coupled equations, which govern the multi-dimensional reactor behaviour, can be solved without exceeding the fast-memory capacity of large computers. In addition, these methods have been tested by comparison of predicted power distributions to experimental data obtained from operating reactors, and thus, considerable experience has been gained in the application of these methods and in the formulation of ways by which they can be tuned to provide acceptable predictions of important reactor quantities.

2.2.2 Advanced nodal methods

Nodal methods with stronger theoretical foundations than the 1-group or $1^1/_2$-group nodal methods in the previous section have been devised over the past fifteen years or so. These more advanced methods rely on systematic procedures for the determination of the additional relations needed between node-average fluxes and surface-average currents. Because of their more systematic and rigorous nature, these advanced nodal schemes provide accurate predictions of criticality and nodal powers, without relying on empirical adjustments. However, a penalty of increased computer storage requirements is often incurred when these methods are utilized (Lawrence, 1986).

The advanced nodal methods typically derive the flux-current spatial coupling equations by decomposing the three-dimensional neutron balance equation in each node into three coupled, one dimensional equations and by solving each one-dimensional equation with an approximate spatial shape assumed for the transverse leakage term. Most nodal methods assume this shape to be quadratic but this is currently the subject of research.

The advanced nodal schemes include the flux expansion method, the nodal expansion method, the nodal Green's function method, and the analytical nodal methods. In this work, one of the most recent advanced nodal diffusion codes, MGRAC (Multi-Group Reactor Analysis Code) will be used to perform the core calculations when evaluating the efficiency and the accuracy of our detector model. A brief overview of this code is discussed in ***Section 2.5*** below.

2.3 Review of Flux Reconstruction Methods

This work will explore the incentive of using flux reconstruction in determining detector responses as this has the advantage of giving an accurate prediction of the flux in the detector position, taking all the heterogeneity into account. Perhaps the simplest approach to reconstruction is the normalization method, in which the heterogeneous power distribution computed for a node with zero-current boundary conditions is re-normalized to preserve the node average power predicted by the nodal solution. Unfortunately, this method cannot account for power gradients across a node and has been shown to be extremely inaccurate in tilted flux conditions (Smith et al, 1980). Another, more accurate reconstruction method is called the modulation method (Koebke et al, 1977). This method corrects the heterogeneous flux (or power) distribution obtained for a node from a zero-current calculation by multiplying it by a smooth nodal flux distribution determined by an interpolation procedure that utilizes information from the homogenized nodal solution.

The third approach to reconstruction relies on imbedded, heterogeneous flux calculations for each node, with boundary conditions for the calculations deduced from quantities output by the nodal solution. The quantities imposed as boundary conditions may be albedos, net currents or fluxes. The shapes of these quantities are typically assumed to be flat, linear or quadratic and are often adjusted to account for local irregularities by using information from zero-current assembly calculations. Although the imbedded calculations

can yield accurate results, they are relatively expensive to implement, since they rely on auxiliary fine-mesh calculations for each node (Khalil, 1983). Furthermore, although response matrix procedures can be employed to reduce the expense of the imbedded methods, the calculation, storage and interpolation of response matrices for different nodal conditions are also relatively inefficient (Smith et al, 1980).

A method for computing detailed information, which relies on the performance of two-dimensional, full core calculations, has also been developed not so long ago. In this method, called PSEUDAX, (Rothleder, et al 1982) the detailed 2-D power distribution obtained for a given radial slice of the core is adjusted to produce node-average powers output for a particular core elevation by a 3-D nodal solution. Although this method accounts in an approximate manner for local feedback effects and for 3-D effects, the required calculation of 2-D power shapes for the full-core is quite expensive.

In this work, the assembly modulation method (Koebke, et al, 1983) will be used to reconstruct the flux distribution in the Koeberg PWR nodes for selected cycles). This method is extremely efficient and is discussed in more detail in the following section.

2.3.1 The modulation method

This method is attractive because of its computational efficiency, since no heterogeneous fine-mesh calculations for the assemblies in situ are required. Instead it is sufficient to pre-compute fine-mesh form functions

$$f_g^{het}(r) = \frac{\phi_g^{het*}(r)}{\phi_g^{\hom*}} \qquad (2.1)$$

for every type of assembly or at most, for clusters involving a few assemblies. $\phi_g^{het*}(\mathbf{r})$ is the flux distribution of the assembly, with all the heterogeneities represented explicitly but

obtained from calculations with approximate boundary conditions. $\phi_g^{hom^*}(\mathbf{r})$ is the solution of the corresponding equivalent homogenised problem for the same boundary conditions. The form function $f_g^{het}(\mathbf{r})$ has the important property that it depends only weakly on the actual boundary conditions. Hence, it is usually determined as a by-product of conventional heterogeneous assembly calculations with zero net current boundary conditions. In that case $\phi_g^{hom^*}(\mathbf{r})$ is constant and $f_g^{het}(\mathbf{r})$ becomes independent of the nodal approximations. On the other hand, if the assembly is homogenised in a typical environment, one must compute $\phi_g^{hom^*}(\mathbf{r})$ using the same nodal approximations as in the subsequent global reactor calculation.

An approximation of the reconstructed flux distribution of the assembly in the global problem is then obtained simply by modulating the global homogenised flux distribution with the heterogeneous form function

$$\phi_g^{het}(r) = f_g^{het}(r) \bullet \phi_g^{hom}(r) \qquad (2.2)$$

Note that equation (2.2) yields the exact heterogeneous flux distribution if the exact boundary conditions would be used as when determining $f_g^{het}(\mathbf{r})$ in equation (2.1). (Koebke et al 1983).

Besides the fact that the modulation method requires the use of consistent methods of homogenisation, the key problem that must be solved is to get good approximations to the 2-dimensional homogenised flux distribution $\phi_g^{hom}(\mathbf{r})$ within the nodes. In the practical case, where the $\phi_g^{hom}(\mathbf{r})$ must be determined from results of nodal coarse mesh calculations this is a difficult problem. Essentially, two different approaches have been investigated in (Koebke et al 1977) namely, the local high order interpolating techniques and the approximate analytical solutions. The use of high order-order polynomials for

interpolating the thermal flux over an entire assembly leads in certain cases to disappointing results.

For a rodded assembly like in the case of Koeberg, the thermal form functions exhibit a transient exponential behaviour near the boundaries. Therefore, one must either use a coarse mesh of 2x2 nodes per assembly or include exponentials in the interpolation functions (Hoxie C et al, 1981). Both the methods require the determination of approximate flux values at the nodal corner points.

The modulation method of determining pin-wise power distributions as described above are in full production use for PWR design calculations and further improvements are anticipated as research in this area unfolds.

From the above theoretical arguments, it is apparent that the development of our detector model must take full cognisance of the theoretical considerations alluded above. It is therefore imperative that our assembly model and description must be within the calculational ability of either of the above-mentioned tools, i.e. advanced nodal methods or flux reconstruction methods, and for the latter, it (the assembly description) must lend itself compatibly and conveniently to the modulation method. A full description of the assembly in which we envisage to apply the above theoretical provisions is given in ***Chapter 3***.

2.4 Transport and Diffusion Theory Codes as used in the Study

As pointed out in ***Chapter 1***, the transport theory provides the basic theory analyzing a nuclear reactor. However, the transport theory equation is too complex in analyzing practical reactors. Instead, a two-step process is required. The first is to compute the cross sections for the various regions of a nuclear reactor and the second step is to employ diffusion theory together with the cross sections to analyze the lifetime, power distribution and other physical characteristics of the reactor. Frequently used cross section generating

codes like WIMS, employ integral transport theory to develop the multigroup cross sections, and diffusion theory codes are derived from the transport equation to analyze the reactor as a whole. The cross section generating codes first assume an infinite array of the fuel assemblies, and consider the motion of the neutron along a straight line.

This work makes use of the above philosophy, in that it uses MGRAC which makes use of diffusion theory method (nodal) for the core calculations and also the HEADE code which uses transport theory principles for both cross section generation and assembly depletion calculations. The details of these codes are given in later sections of this dissertation.

2.5 The MGRAC Code

2.5.1 Overview

MGRAC, the Multi-Group Reactor Analysis Code is a modern nodal diffusion code which has been developed by NECSA (formerly the Atomic Energy Corporation of South Africa) and forms part of the OSCAR-3 calculation system (Muller et al. 1994). Nuclear reactors with Cartesian geometry can be modelled in one, two or three dimensions with no restriction on the number of neutron energy groups used. Non-linear feedback is used to include the effect of physical core conditions on cross sections.

2.5.2 Summary of MGRAC features

MGRAC utilizes a quasi-static approach to model the long-term depletion behaviour of a reactor core: static diffusion theory calculations at selected time points determine the flux/power levels for the solutions of the time-dependent depletion equations over broad time steps (burnup steps). A sophisticated cross section model is incorporated to cater for power and burnup-dependent feedback (Reitsma, 1999). A simple closed-channel thermal-hydraulic model for PWR calculations forms part of MGRAC and is used to determine the fuel and moderator temperature. The cross sections are read from a

quadratic polynomial cross section library and are available as a function of burnup, fuel temperature, moderator temperature and density and boron concentration. Using the data on this polynomial cross section library, a range of criticality searches can be performed: control rod, power, soluble boron (for PWRs) and inlet conditions. The cross section model as used in this work is based on a microscopic representation (i.e. isotopic cross sections), which is compatible with a microscopic depletion approach. In the microscopic depletion model implemented in MGRAC the isotopic depletion equations are solved analytically, thus providing an exact solution to the isotopics subject to the physical assumption that the flux spectrum and the flux/power level remain constant during the burnup steps. In MGRAC, the diffusion equation is solved in an arbitrary user-specified number of energy groups using either a standard mesh-centred finite-difference method or an advanced analytical nodal method. The nodal method as explained earlier in the text, is a very accurate and efficient coarse-mesh method, which is specifically geared for applications in which whole assemblies have been homogenized in the radial dimension.

The basic calculational philosophy used in MGRAC is that of stacking "calculation cases" to simulate changing reactor conditions. Each calculational case is representative of a given reactor state such as that associated with a specific burn up step, for example. A sequence of calculational cases can then be used to model a reactor cycle, including various control rod positions. This philosophy will be used in this work to perform core follow calculations for the KOEBERG reactor for selected reactor cycles, so as to test the accuracy of our detector model against plant data. In this way, the exact conditions (burnup, control bank position, inlet temperature and cycle exposure) can be simulated.

2.5.3 A brief Description of the HEADE Code

The assembly modelling in this work was performed using the Heterogeneous Assembly Depletion Code (HEADE). In this code, response matrices for individual fuel cells are

calculated using Carlvik's method (Carlvik, 1967) with the cells cylinderized according to Askew's prescription (Askew, J.R. 1972). The response matrices for the rectangular cells used for the inter-assembly water gaps are synthesised from 1-D collision probability results. Resonance shielding calculations are performed for each fuel pin and separate energy group dependent Dancoff factors are calculated for each fuel pin (based on the nature of its eight nearest neighbour cells). An analytic method (Joanou G.D. et.al, 1964) is used for solving the depletion equations.

The final output of the HEADE code includes homogenized few-group cross-sections, face discontinuity factors and form factors (for power and flux). Microscopic cross sections are prepared for a user-specified list of isotopes. The remainder of the isotopes and materials are collected in a single structural material. The microscopic cross section treatment is restricted to the normal reaction cross-section types (capture, fission, and scatter) and specifically excludes transport cross sections. The transport cross section is allocated to a macroscopic material and is defined as a mixture macroscopic cross section related to an assembly diffusion coefficient via the standard $\Sigma_{tr}=1/(3D)$ formula. The few-group diffusion coefficients are computed in two stages. First, multi-group flux-volume weighted homogenized macroscopic transport cross sections are computed for the assembly. Second, the diffusion coefficients derived from these multi-group transport cross sections are flux-collapsed (using the assembly-average spectrum) to the desired few-group structure.

2.6 Conclusion

In this chapter, an in-depth investigation of nodal methods in reactor analysis was done. Due consideration was given to the modern nodal methods because they form the basis of this work. It was stated that the emergence of these methods have tremendously eased the work of a reactor physicist because they brought with themselves, an incentive of

performing core calculations in a more reliable and less time consuming way, compared to the earlier nodal methods. Testimony to this is the state-of-the-art MGRAC code whose user-friendliness will show the robustness and the flexibility but yet accurate manner in which nodal methods perform core analysis.

CHAPTER 3 ASSEMBLY DESCRIPTION.

3.1 Assembly modelling using HEADE

The work on the modelling of the different assemblies of the Koeberg reactor have been done by the reactor theory group of the Atomic Energy Corporation of South Africa and the information used here has been obtained from the Koeblib 3.0 report (AEC Report PIN 1331).

The assembly depletion calculations were performed with the HEterogeneous Assembly DEpletion code (HEADE), which is based on a low-order (double-P_0 angular and flat spatial distribution of interface flux) interface current formalism (Joubert, W.R. 1992). The basic nuclear data used by the HEADE code is derived from the 172-group WIMS nuclear data library (Taubman, C.J., 1975). Cross sections for the gadolinium isotopes were generated from ENDF-B/6 data (Rose P.F. et al.1990) with the NJOY package (Macfarlane R.E. et al 1993).

The cross section data utilized in HEADE is a fine group library. This fine-group data cannot be used directly to do the core calculations because of the core size. However we note that the reactor core have a regular or periodic lattice structure in which one sub-element is repeated throughout the core, for example, a fuel pin or a group of fuel pins can be regarded as a unit cell.

The essential scheme then is to perform a detailed calculation of the flux distribution in an assembly; (usually assuming that there is a zero net neutron current across the boundary of the cell). The various multi-group cross sections characterizing materials in the assembly are then averaged spatially over the assembly using the flux distribution as a weighting function (Duderstadt et al,1976). This scheme essentially replaces the actual

unit cell by an equivalent homogenous unit cell characterized by these effective cross sections.

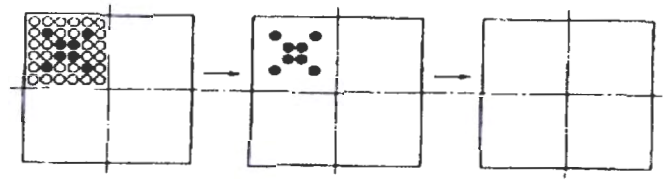

Figure 3-1: Fuel Assembly Homogenization

The flux we calculate from HEADE is a function of space and energy i.e. $\phi(r,E_g)$. With HEADE, we average the cross sections and homogenize them, i.e. the energy range averaged from 172-energy group to just 2 groups. In this way, we can summarily note that homogenization implies, averaging the cross sections over space while group collapsing will imply averaging the cross sections over energy (Sesonske A. et al. 1963) i.e.:

$$\Sigma_g = \frac{\int_v d^3r \Sigma_g(r)\phi_g(r)}{\int_v d^3r \phi_g(r)} \qquad \text{homogenisation}$$

and

$$\Sigma_G(r) = \frac{\sum_{g\in G} \Sigma_g(r)\phi_g(r)}{\sum_{g\in G} \phi_g(r)} \qquad \text{group collapsing}$$

Or combined we get:

$$\Sigma_G = \frac{\int_{Eg}^{E'g} dE \int_v d^3r \Sigma_g(r)\phi_g(r)}{\int_{Eg}^{E'g} dE \int_v d^3r \phi_g(r)}$$

The cross section data calculated by HEADE is given in terms of homogenized few group cross sections which we need to perform core calculations for the KOEBERG reactor. Finally, the multi-group three-dimension nodal diffusion code called MGRAC will then be used to determine the flux and power distribution in such a reactor core.

In addition to the homogenized cross sections, HEADE was also used to calculate the few group microscopic ^{235}U fission cross sections, also called the detector constants in this work. These are in turn used to predict detector responses in different detector positions in the core and hence the results can be compared relatively to the actual plant data (measurements). Note that only the assembly- averaged quantities are obtained from the nodal diffusion solution in MGRAC and that the fission rates in the detector positions are not calculated directly. We therefore need a detector model in order to establish a more reliable way to compare our results with plant data and in that way validate our calculation model. In this work, only fission detectors are considered and therefore the detector constant always refer to the ^{235}U microscopic fission cross section.

3.2 Physical Characteristics

The physical data defining the geometry and material composition of the fuel assemblies are given in the ***Appendix A***. The processing of this engineering data into the format needed for an assembly calculation forms a major part of any assembly code and is mostly still lacking in HEADE. Many computations (such as thermal expansions and axial smearing of grid materials) must be done before hand. The derived physical conditions resulting from this pre-processing and used in the assembly calculations are given in ***Appendix B***. These calculations were performed at base conditions only, as will be explained in ***Section 3.3*** below.

The assemblies were modelled in 2-D with heterogeneous pins and an explicit inter-assembly water gap. Some of the structural elements such as spacer grids and sleeves were smeared into the appropriate regions. Where applicable, geometrical variations to the system such as control rod insertion and burnable poison extraction were explicitly modelled. This two-dimensional assembly model is made up of a number of spheres in which the fuel, control and burnable poison rods as well as the guide tubes structural material and inter-assembly water gap are represented.

Assembly calculations were performed for UO_2 fuel of five different enrichments (1.8, 2.4, 3.1, 3.25 and 3.9 wt %) Some assemblies contained removable boro-silicate burnable poison rods. In one case 0.4 wt% UO2 pins containing gadolinium replaced some fuel pins. The Gadolinium loaded pins were assumed to contain 8wt% Gd_2O_3 homogeneously distributed in the UO_2 matrix (Reitsma F. et al, 2000).

It must be noted that the assemblies loaded with burnable poisons were for start-up cycles of KOEBERG. The purpose of having these burnable poisons loaded may be summarised as follows:

The lifetime of a given core fuel loading i.e. the period during which the core has sufficient excess reactivity to permit start-up and full power operation, is generally determined by the amount of fuel initially loaded into the reactor core. In order to increase allowable initial core fuel loading, it was important to load into the core materials characterised by high neutron-absorption cross sections (poisons) that compensate for excess reactivity during the early stages of core life. Such absorbers are chosen such that they 'burn out' somewhat faster than fuel burnup, so that later in the core life they contribute negligible negative reactivity (Duderstadt J, et al, 1976). The fuel assembly types in KOEBERG are

all uniquely defined by their enrichment and burnable poison loading, details of which are given in ***Table 3-1*** below.

The fuel assembly names or ID's are fully descriptive in so far as fields in the name are reserved for different properties. For example W170310B016- in ***Table 3-1*** below denotes a Westinghouse type PWR assembly with a 17x17-fuel pin lattice. The uranium is 3.10% enriched and Boron burnable poisons rods are placed in 16 positions in the assembly.

Table 3-1: Assembly Types in the Koeberg Core

Assembly ID	Enrichment	Burnable Poison Loading
W170180-000-	1.80 %	0
W170240B008-	2.40 %	8
W170240B012-	2.40 %	12
W170310-000-	3.10 %	0
W170310B012-	3.10 %	12
W170310B016-	3.10 %	16
W170390G012-	3.90 %	12 (Gd)

3.3 Base/Off-Base Scheme

The generation of the nodal equivalent parameters (cross sections, discontinuity factors, etc.) for the cross section library is performed using a base/off-base calculation philosophy. Assembly depletion calculations are normally performed at average operating conditions, known as the base conditions. The set of parameters defining the condition of the system is referred to as the state parameters. At each depletion point (time step) of the depletion calculation auxiliary (non-depletion) calculations, known as off-base calculations, are performed with one of the state parameters varied from the base value to determine the influence of the state parameter on the nodal equivalent parameters.

Cross sections are generated for each type of assembly at various state parameter conditions and within the OSCAR-3 code system, these are then fitted by polynomials as functions of the state parameters to give the final polynomial cross section library. When generating these cross sections it is assumed that the state parameters can be varied independently, that is, one state parameter can be modified while keeping the rest fixed at their base values.

The state parameters used for the KOEBERG library are exposure, fuel temperature, moderator temperature and soluble boron concentration. Assembly parameters such as power, temperatures etc. are kept constant during the depletion calculation. Off-base calculations are performed at each burn-up step for variations in soluble boron concentration, fuel temperature and moderator temperature. Moderator density is changed along with the moderator temperature according to a given moderator pressure. However, the water density and temperature may be de-coupled, although it was not done for this work. It should be noted that a uniform fuel temperature and a uniform water temperature are used (no spatial temperature variation across an assembly). Xenon number densities were allowed to evolved naturally - no enforced equilibrium - and were also not adjusted when fuel temperature (power) was changed. The spectral effects of Xe should actually be taken into account by having Xe number density as state parameter.

The entire sequence of off-base calculations is repeated for possible geometrical variations before proceeding to the next burnup step. This includes the extraction of the burnable poison rods for all assembly types loaded with burnable poisons. A provision has also been made for the insertion of control rods into all assembly types. Obviously control rods can only be inserted into burnable poison loaded fuel assemblies once the burnable poison rods have been removed since these all have to occupy the same position in the assemblies. Parameters characterising this scheme are represented in table 2 below.

Table 3-2: Base and Off-base Conditions

Base Conditions		
Pressure	155 bar	
Power density	183 W/cm	
Moderator Temperature	306.3 °C	
Fuel temperature	Function of burnup	
Boron Concentration	600 ppm	
Off Base Variation		
Moderator temperature	+ 15 °C	- 15 °C
Fuel Temperature	+ 200 °C	- 200 °C
Boron concentration	+ 600 ppm	- 600 ppm

A vital aspect of this calculation scheme is the modelling of the thermal hydraulic behaviour of the assemblies at the various base and off-base conditions.

In order to determine the sensitivity of the detector to its environment the effect of changes in the state parameters (or reactor conditions) on the ^{235}U microscopic fission cross sections were compared to see which parameter variations are worth considering in our detector models and the extent of their effect. Using this scheme for every assembly type, the effect of change in boron concentration, fuel and moderator temperature for when the control rods were inserted, not inserted and for the case when burnable poisons were extracted was investigated. This was quantified by plotting the detector constants (^{235}U microscopic fission cross-sections) as a function of burnup /depletion). The resulting graphs from the above procedure are found and described below.

3.4 Results of the detector sensitivity as a function of reactor conditions

3.4.1 The detector constant as a function of burnup at base conditions

In ***Figure 3-3***, the one group detector constant as a function of burnup is presented in a graphical form. It is observed from this graph that the detector constant ($^{235}U\ \sigma_f$) decreases considerably with burn-up at the beginning of the cycle up to a certain value around 18000 MWD/te and then remains fairly constant. This observation and trend is evident in all assemblies without regard to their off-base status (i.e. whether or not off-base parameters are varied).

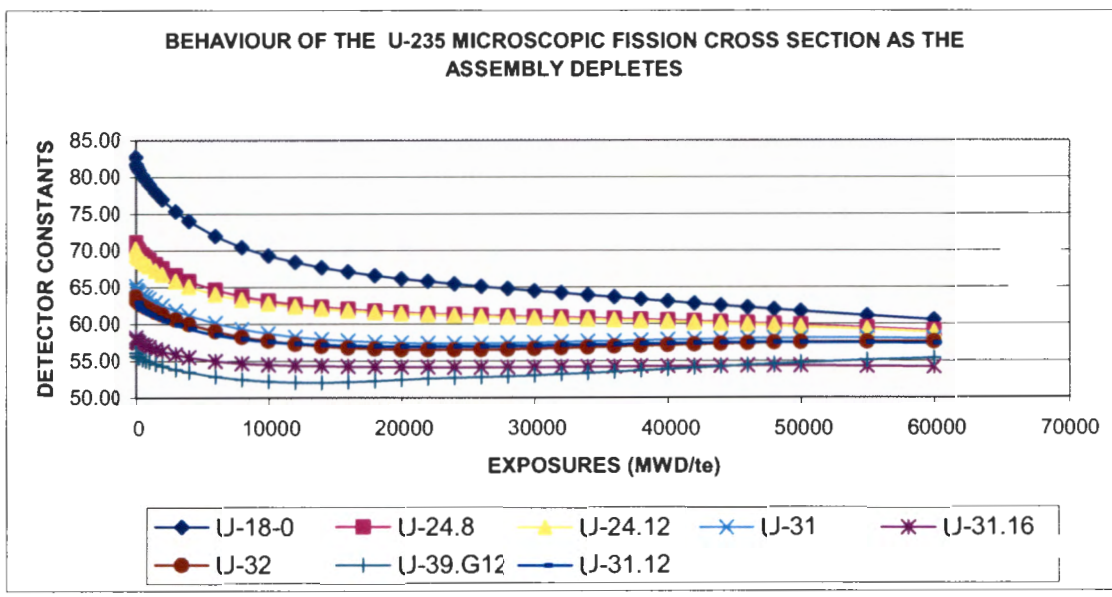

Figure 3-2: Behaviour of the detector constant as a function of burnup

A close scrutiny of the graph also shows a small but drastic "jump" at the beginning of the cycle, say at around 1000 MWD/te, which is due to the build-up of a fission product, Xenon. This however does not last for long because Xenon is a short-lived fission product and burn out quickly. The subsequent decrease of the ^{235}U as a function of burnup is due to longer-lived fission products and the plutonium build-up as uranium continues to deplete. This then, will cause energy spectral changes and since there is a relative change in the flux spectrum distribution, the weighting factor will also change. These spectral

changes are derived from the fact that the microscopic fission cross-section values used were collapsed from 172 groups to just one group. Since the flux at the beginning of the cycle varied until at around 18000 MWD/te this had an effect on our averaged cross sections i.e.:

$$\text{In } \sigma_f = \frac{\sum \sigma_f \phi_g(r)}{\sum \phi(r)}$$

if ϕ_g changes, then σ_f will also change.

After 18000 MWD/te the microscopic fission cross section remains fairly constant because now the flux spectrum has reached a stage where it stays relatively constant. At this stage, the build-up of plutonium (resulting from the burnup of uranium) have reached equilibrium and hence the flat shape of the graph.

3.4.2 Response of the detector constant to different assembly types (base conditions

This phenomenon was evaluated for two categories of assemblies namely; enriched assemblies with burnable poisons loaded and enriched assemblies with no burnable poisons loaded. Assemblies of different enrichment were compared. A distinction was also made for the situation when control rods were inserted.

3.4.2.1 Assemblies with various enrichment with no burnable poisons

For Koeberg, the assemblies with no burnable poisons are those with 1.8%, 3.1% and 3.2% ^{235}U enrichment. (refer to assembly pictures in the appendices).

For assemblies of these types, we observe that the ^{235}U microscopic fission cross section is inversely proportional to percentage enrichment.

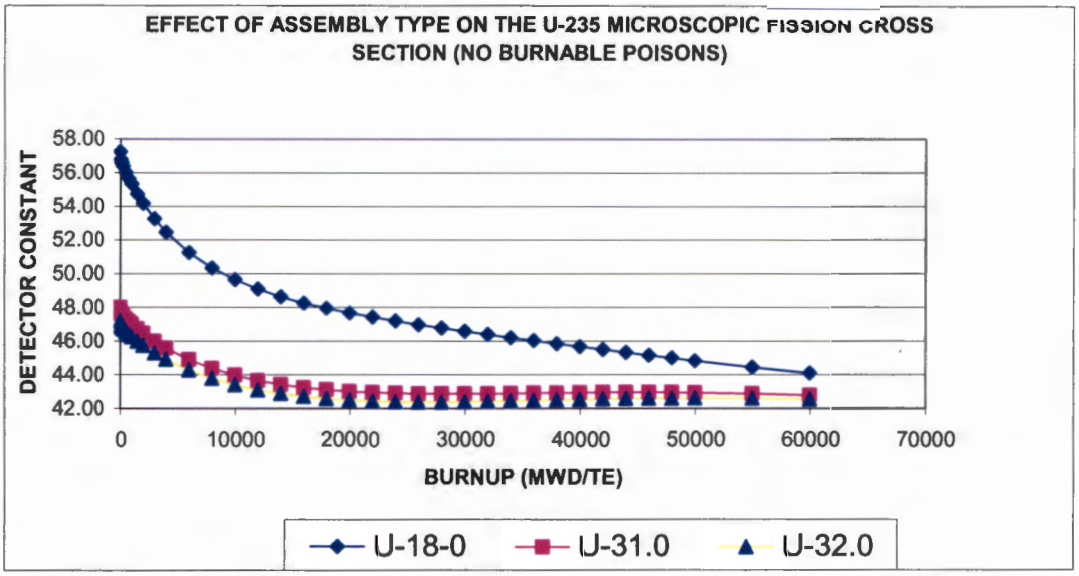

Figure 3-3: Behaviour of the detector constant in different assembly types (no BPs

To illustrate this, we note from the graph (***Figure 3-4***) (that ^{235}U σ_f for a 1.8%, enriched assembly is considerably higher than for the 3.1% and 3.2% enriched assemblies. It must be noted that fission rate depends on the number density of ^{235}U and the fission cross-section of ^{235}U and hence this effect is due to the combination of these two factors. As enrichment increase, there is less slowing down effect (less ^{238}U atoms) but increased thermal absorption through ^{235}U spectrum and this causes spectral changes.

3.4.2.2 Assemblies of various enrichment and with burnable poisons

Assemblies of this type at Koeberg are the 2.4% enriched, 8 pins loaded with burnable poisons, 2.4% enriched, 12 pins loaded with BP's, 3.1% enriched, 12 pins loaded with BP's, 3.1% enriched, 16 pins loaded with BP's and finally, 3.9% enriched, 12 pins loaded with gadolinium. It must also be noted that for the latter assembly type, a special poison, Gd, has been introduced. This poison presents a more advanced fuel design than the burnable poison rods that are used on other assembly types because of its unique properties, notably its high microscopic absorption cross section on the thermal region (about 49000 barns at 0.0253 eV) and its density of 7.95 g/cm^3 and also that it is mixed

with fuel, unlike Boron-10 (whose σ_a at 0.0253 eV is 3837 barns) which is loaded in separate pins on its own.

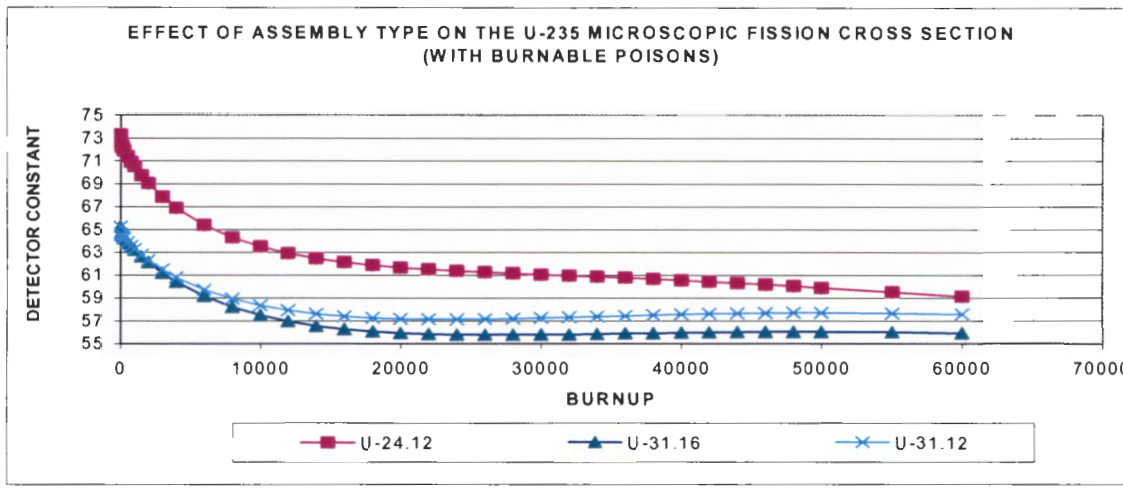

Figure 3-4: Behaviour of the detector constant in different assembly types (with BPs)

For this scenario, it is observed from the graph in figure 3.4 that the same trend as in the previous case above regarding enrichment still holds, i.e. enrichment is inversely proportional to ^{235}U fission cross section (the detector constant). However there is also an additional observation and trend, namely that the number of positions in which the burnable poisons are loaded is also inversely proportional to the ^{235}U σ_f. To illustrate this from the graph, we notice that the lesser the number of positions loaded with burnable poisons, the higher will the detector constant value be. (cf. 2.4% enriched 8 BP's with 3.1% enriched, 16 BP's from the graph in ***Figure 3-3***).

To explain the phenomenon in figure 3.5, we need to briefly recap on the role of burnable poisons in reactor control. Considerably more reactivity control is required before start-up of a new core, which is clean, cold and loaded with fresh fuel, and during the early stages of the operation of the core, than is needed towards the end of core life. In order to reduce these control requirements, it is common to place at selected locations in the core a burnable poison. This is a nuclide that has a large absorption cross section which is

converted into a nuclide with a low absorption cross section as a result of neutron absorption. (Gladstone, S and Sensonske, A.: 1981) From this recapitulation, it becomes obvious that those assemblies with a higher number of pins loaded with burnable poisons will have a low ^{235}U σ_f because the burnable poisons will absorb thermal neutrons which are need to induce more fission reactions, thereby resulting in a less probability for fission to occur or in other words, a harder spectrum will result.

3.4.3 Response of the detector constant to different assembly types when control rods are inserted

3.4.3.1 Assembly types with no burnable poisons

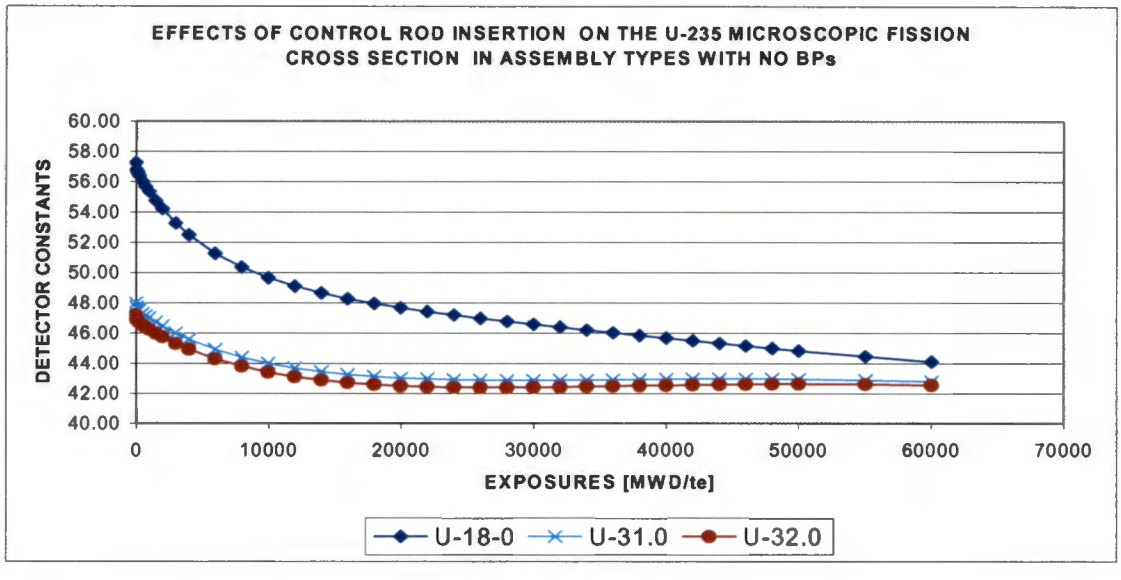

Figure 3-5: Behaviour of the detector constant when control rod are inserted (no BPs)

Generally for all the assemblies with no burnable poisons, the detector constant is reduced significantly as a result of insertion of control rods. The decrease in ^{235}U σ_f as a result of insertion of control rods is obviously because the control rods are made of materials characterised by high thermal neutron absorption cross section i.e. Ag-In-Cd alloy, (where Ag and In have lower thermal σ_a values of 63 and 191 barns respectively and with the

ability to absorb neutrons in the epi-thermal region and Cd having the highest σ_a value of 2450 barns at 0.0253 eV) and will therefore absorb thermal neutrons, resulting in a harder spectrum and less probability for ^{235}U fission to occur.

3.4.3.2 Assembly types with burnable poisons

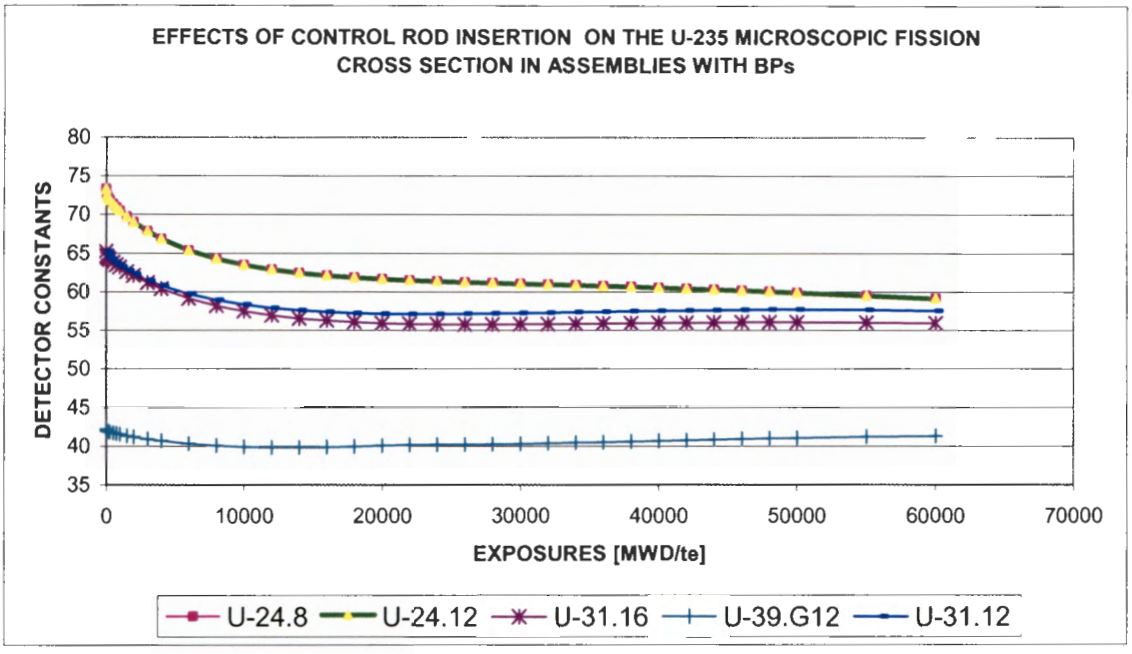

Figure 3-6: Behaviour of the detector constant when control rods are inserted (assemblies with BPs)

It must be noted that burnable poisons and control rods have a similar effect in reactor control. Burnable poisons reduce the number of control rods required in reactors that use control rods for control due to their ability to allow the excess reactivity that is needed to achieve the cycle length. It is therefore imperative to realise that in this case, when control rods were inserted, burnable poisons were extracted, and that the same effect that we observed for control rods was also realised for burnable poisons except for the case of the assembly with gadolinium poison (fig 3.7). The behaviour in this particular assembly is to the effect that the ^{235}U microscopic fission cross section is quite low because of the uniquely high σ_a value for gadolinium at thermal energies, thereby effecting spectral changes.

3.4.4 Off base conditions

As mentioned earlier in this chapter, the one group detector constant was calculated for certain reactor conditions that were then referred to as off-base conditions. These conditions are those that were used to predict how the detector constant (the ^{235}U fission cross section) will behave when certain core parameters are varied for one reason or another e.g. during accidents or reactor experiments etc. The parameters of interest were chosen to be the temperature of the moderator, temperature of fuel and the concentration of boron. Each of these parameters was varied by equal amounts on the negative and positive side of the base conditions i.e. the moderator temperature was varied by plus and minus 15 K, the fuel temperature by plus and minus 200^0C and the boron concentration by plus and minus 600 ppm. The resulting detector response is discussed in the following sections.

3.4.4.1 Response of the detector constant to moderator temperature variations

The temperature of the moderator is one of the state parameters that were identified to evaluate the sensitivity of the detector model in this work. Obviously, this parameter must have an effect on the detector model because of the role of the moderator in the operation of the reactor, i.e. to slow down / thermalize neutrons. In this study, this parameter was varied by plus and minus 15 K and the resulting detector response was presented graphically as shown in ***Figure 3-8***. This graph actually depicts the scenario for a U-2.4, 8 BPs assembly type and it is representative of all assembly types because the trend we observe here holds for all other assemblies. From this graph, the general trend is that when the moderator temperature is increased or decreased, there is an equal but opposite effect on the detector constant. Basically, an increase in moderator temperature leads to the decrease in moderator number density. Reducing the moderator number density produces two thermal effects; viz. it reduces the thermal absorption, and it hardens the

thermal spectrum. The first is a positive feedback and can be large if a high concentration of soluble boron is in the moderator. The spectral hardening for uranium cores is a negative reactivity feedback and it is usually small. This is because when the moderator temperature increases the density of the water decreases and the reduction in the moderator density causes a reduced slowing-down effect, (for under-moderated systems) the neutrons flux spectrum becomes harder.

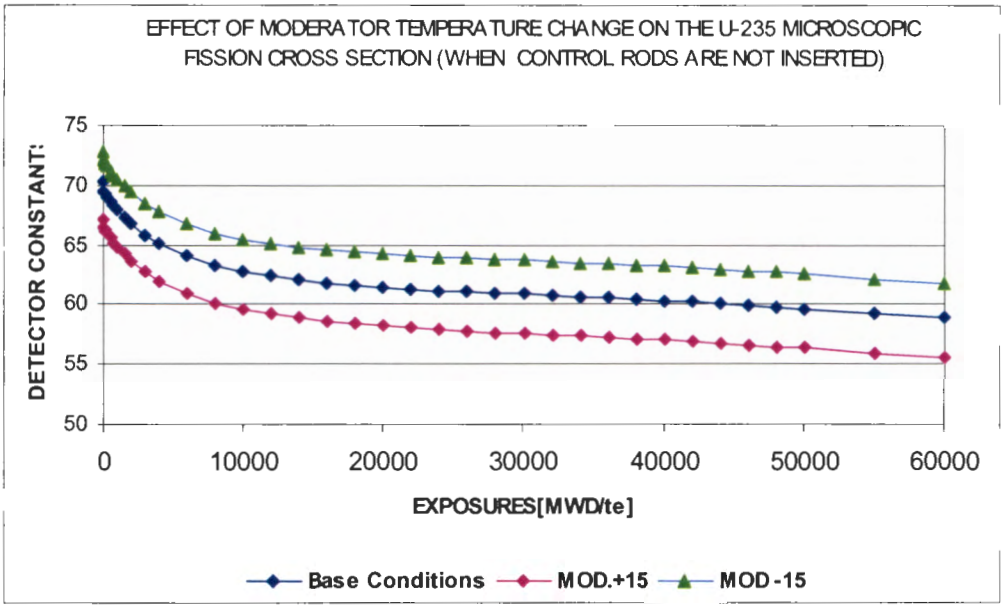

Figure 3-7: Behaviour of the detector constant when moderator temperature is varied

Likewise, when the moderator temperature is decreased, the water density will increase and this will result in an increased slowing-down effect and hence a softer spectrum in the reactor. Changing the moderator temperature also affects the resonance escape probability and fast leakage which are the other two parameters contributing to the moderator temperature coefficient but these are obviously of little significance to the spectrum change.

3.4.4.2 Response of detector constant to boron concentration variations

An increase in the Boron concentration will effect a low microscopic fission cross section of ^{235}U because due to its high microscopic absorption cross section in the thermal region, a more concentrated Boron will absorb more thermal neutron and thereby resulting in the

hardening of the spectrum, hence there will be few neutrons left to induce fission. This will harden the spectrum and thus decrease the effective one group ^{235}U σ_f as seen in ***Figure 3-8*** below.

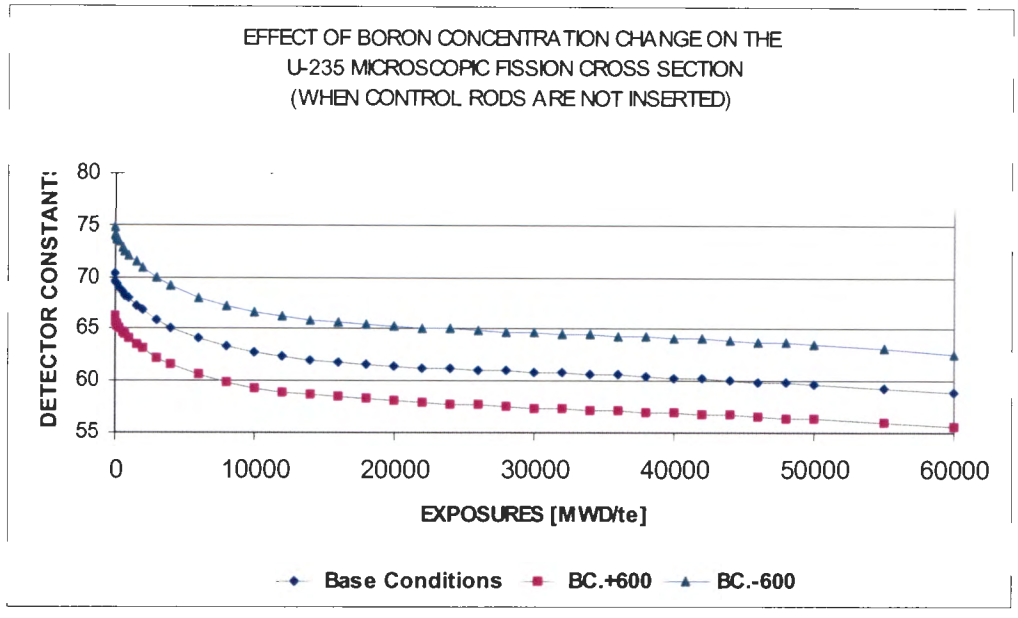

Figure 3-8: Behaviour of the detector constant when boron concentration is varied.

It must also be noted that any variation on the concentration of Boron can have a more profound effect on our detector constant than the burnable poisons loading, because the latter is concentrated at specific positions some distance from the central instrumented thimble, whereas the former is dissolved in the water that surrounds our detector i.e. local versus global effect.

3.4.4.3 Response of the detector constant to fuel temperature variations

The general observation in as far as this parameter is concerned is that a negative prompt reactivity coefficient associated with fuel temperature arises from the Doppler broadening of the resonance in ^{238}U. This will always result in an increased ^{238}U capture with increasing fuel temperature and hence, a decrease in reactivity. The water at the periphery of the fuel slows down neutrons significantly and hence the capture cross section in the fuel is increased, thereby resulting in a harder spectrum. This therefore accounts for the

decrease in the detector constant when temperature is set to +200 °C and the increase in the detector constant when temperature is set to -200 °C as can be seen from the graph below. Again, this graph is for the U2.4, 8BPs-assembly type and the same effect is observed for all other assemblies.

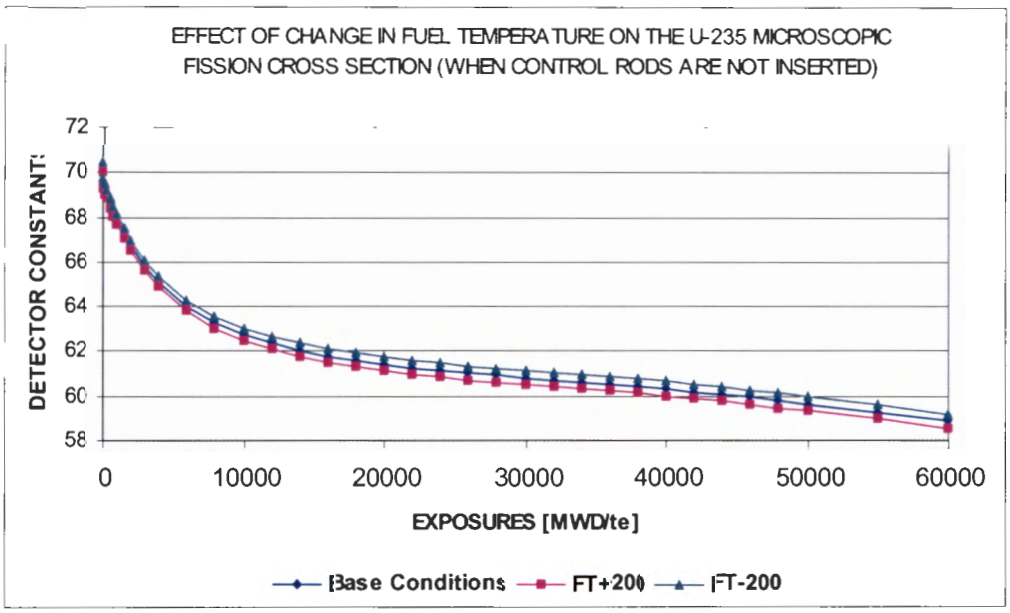

Figure 3-9: Behaviour of the detector constant when fuel temperature is varied

However, the difference in the behaviour of our detector constant when fuel temperature is increased or decreased differs very slightly (about 0.333 barns). This means that the so-called base and off-base conditions of our detector model differs very slightly in this particular parameter. This then tells us that this parameter has very little influence on our final detector model and the effects of its variation therefore can probably be ignored.

3.5 Analysis of the sensitivity of the 2 group detector constant

In the results discussed thus far, the calculations done in HEADE for the preparation of detector constants were collapsed to one group ^{235}U microscopic cross section. This resulted in the sensitivity analyses and the graphs discussed above. An alternative idea was to study the behaviour of the 2-group detector constants or in other words using the two-group microscopic ^{235}U fission cross-section i.e. the fast group and thermal group

respectively. From this we should be able to decide which energy range dominates the overall behaviour of the detector constant as a function of exposure and also its sensitivity to the off-base conditions. Three representative assembly types (viz. the U-3.1%, with 16 BPs, the U-3.25% with no BPs and the U-3.9% with 12 Gd pins) were selected for this purpose. These assembly types were ideal for this purpose because they represented the variety (or the three types) of assembly types studied in this work. In doing this, we recall that our weighted average cross section is given as:

$$\sigma = \frac{\phi_1 \sigma_{f_1} + \phi_2 \sigma_{f_2}}{\phi_1 + \phi_2}$$

where ϕ_1 and ϕ_2 denotes the flux for the fast and thermal range respectively, and σ_{f1} and σ_{f2} denotes the microscopic fission cross section for the fast and thermal range respectively. Two graphs were drawn from the data obtained for the fast and the thermal group so as to quantify the differences between the sensitivities of the detector constants to different assembly types for the two energy groups respectively. Figure 3.10 shows the variations of the base conditions of the detector constant (fission cross section) for the three assembly types above as a function of exposure for the fast group and figure 3.11 shows the same effect but for the thermal group.

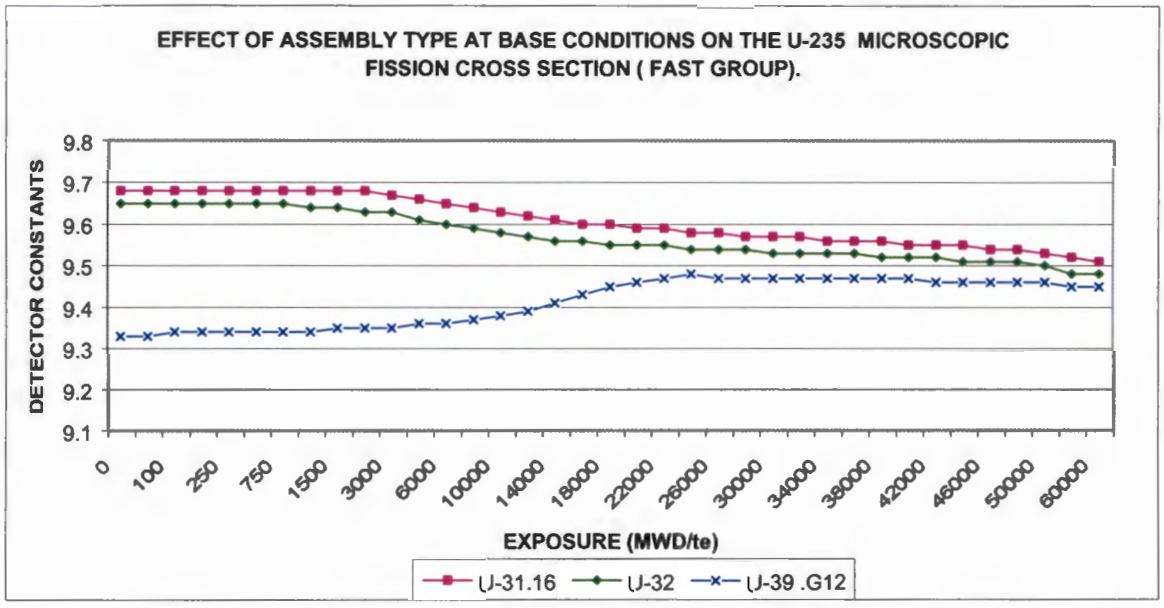

Figure 3-10: Behaviour of the detector constant at base conditions of different assembly types (fast group)

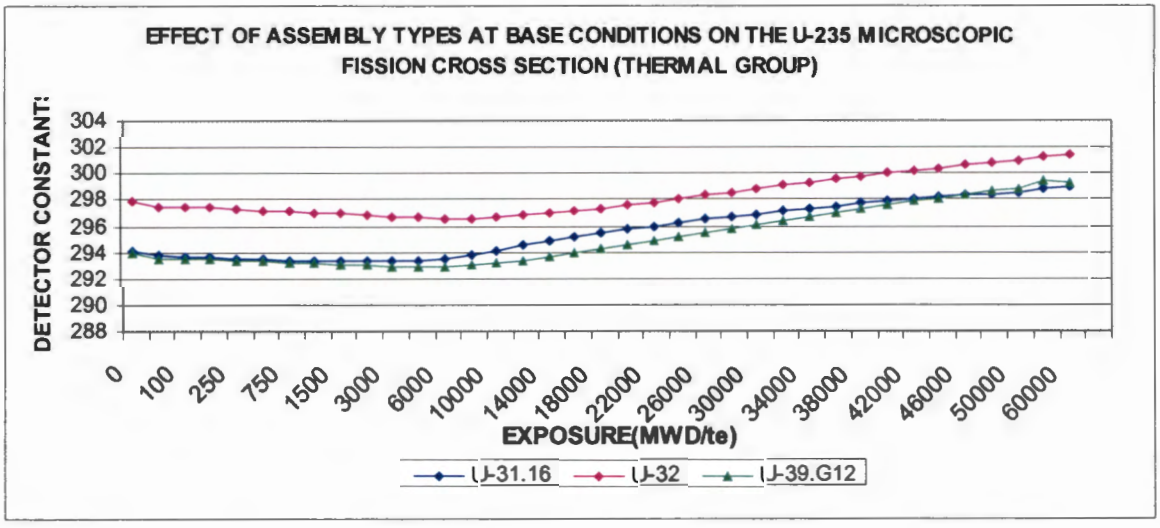

Figure 3-11: Behaviour of the detector constant at base conditions of different assembly types (thermal group)

It was realised that from the graphs above, the two group cross sections are relatively constant (varying with about 1.5% for the thermal range and about 10% for the fast range) as a function of exposure over the burnup range of 0 - 32000 MWD/te whereas the one

group cross-section had a larger variation with exposure (with about 9 barns or ~15%) over the same burnup range. Since the two-group cross sections are relatively constant with exposure, we can conclude from the above equation that the larger variation in the averaged (one group value) cross-section is due to the spectrum changes (i.e. the fast to thermal flux ratio as a function of burnup).

From the above observation it could perhaps be acceptable to assume that the 2-group cross section is independent of the exposure and hence we may choose to store a single set of microscopic 2-group cross sections that is representative of all the 36 exposure points.

Since the cross section in the fast region contributes a small portion to the reaction rate, we may also choose to store only the thermal cross section in calculations/final detector model especially since the fission reactions occurs mostly in the thermal range. When these adjustments are made, we can still expect reasonable accuracy (say < 5% to accommodate both operational and measurement uncertainties) in the predicted detector constants.

Over and above these observations, we note also that there is a marked lack of sensitivity to changes in parameters such as the fuel temperature and to a certain extent, boron concentration by the fast group detector constant, and in such a situation, taking this fast group cross section into consideration in our final detector model will not contribute to the accuracy of the model. Although the fast group respond significantly to changes in moderator temperature, it is also unimportant to consider this response because it is quite small (about 30 times smaller compared to the thermal one).

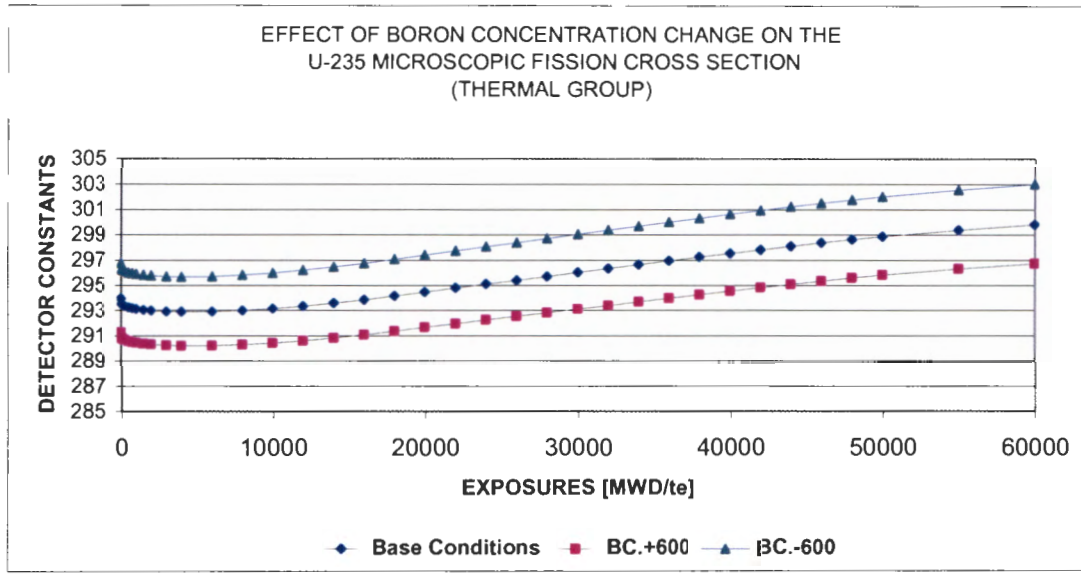

Figure 3-12: Sensitivity of the thermal detector constants to Boron concentration variations

It can also be noted again that the change in the behaviour of the detector constants that we see in the thermal group could be much smaller than the values given here, since the off-base variations were chosen to be larger than will realistically be seen during practical reactor operation. This means that the envisaged accuracy i.e. 5% can easily be accomplished if less extreme off base variations were chosen. However we must note that the rationale behind choosing these extreme values is to ensure that they accommodate all operational conditions of a reactor, (i.e. to interpolate between values instead of extrapolating, which gives less accurate results in our reactor values.) Graphs in ***Figure 3-12*** to

Figure 3-14 show the sensitivity of the thermal group towards off-base variations and the trend as described above is fairly explicit. These graphs are for the U-24.3BPs assembly type and they are representative of all the other assembly types at typical burnup ranges of 0 – 3200 MWD/te since the trend depicted here is similar to that of all other assemblies.

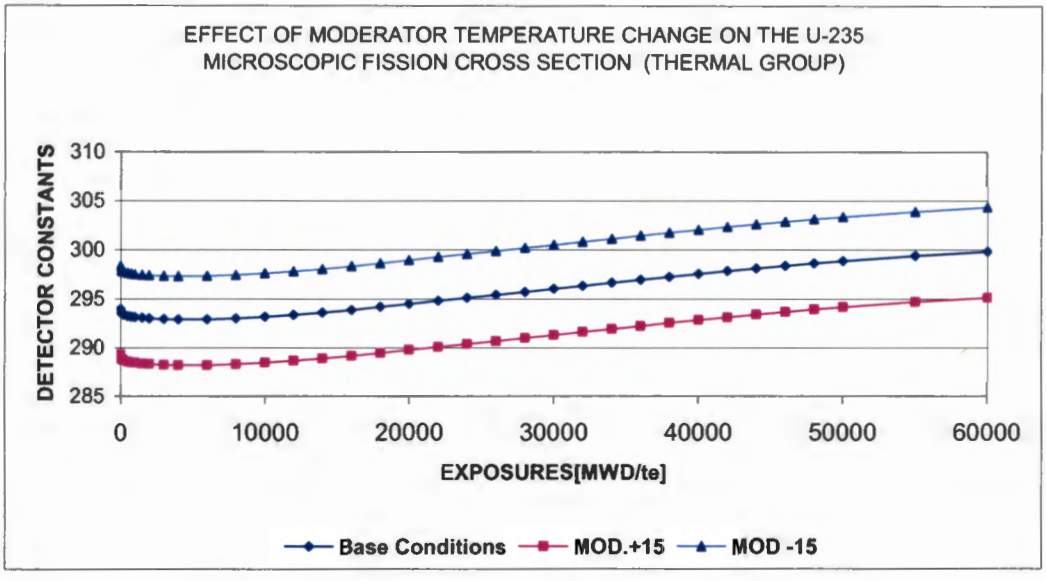

Figure 3-13: Sensitivity of the thermal detector constants to moderator temperature variations

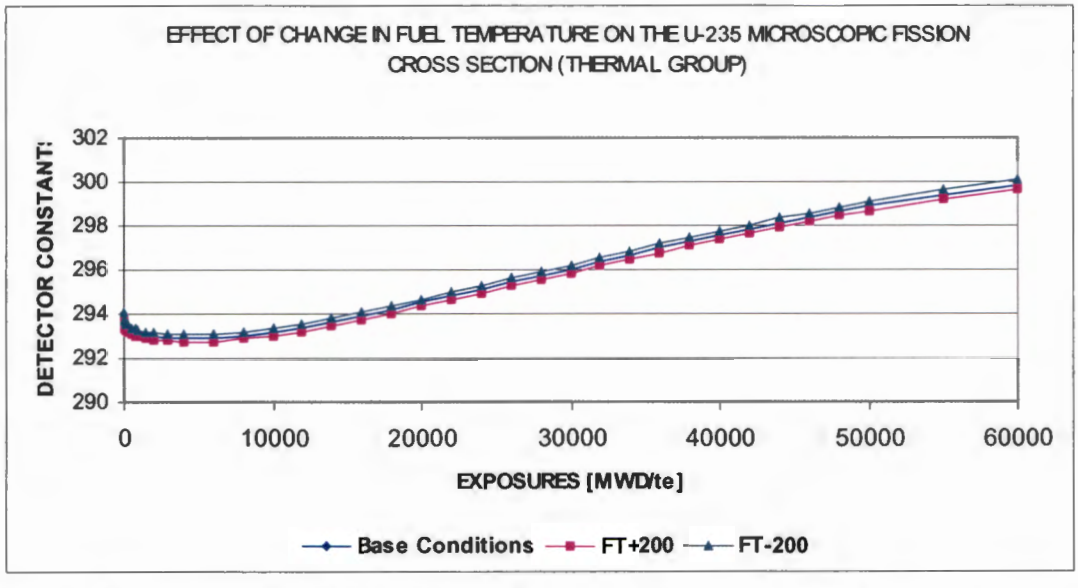

Figure 3-14: Sensitivity of the thermal detector constants to fuel temperature variations

CHAPTER 4 ASSEMBLY / CORE CALCULATIONS AND RESULTS

4.1 Introduction

In the preceding chapter, the reactor specifications, including the fuel and assembly description were given. The codes used to model the above were also described and explained in-depth. A detailed interpretation of the behavior of the detector constant when certain core parameters were changed was also given. Following the above, assembly calculations were performed for the two group detector constants (from the HEADE code), taking all variations into consideration, i.e. detector constants are available as a function of all off-bases and of burn-up. Since a HEADE calculation is done for each assembly type, the detector constants will naturally be available for each.

4.2 MGRAC Core Follow Calculations

Figure 4-1: Assembly-averaged flux model of calculating reaction rates

In performing the core calculations using the MGRAC code, two options were considered to calculate the detector responses, namely, utilizing the assembly averaged flux with the two group detector constants to get the detector fission reaction rate (i.e. the flux of all

positions in the assembly as in ***Figure 4-1***) or utilizing the reconstructed flux (the heterogeneous flux) in the detector positions (i.e. the flux at the center of the assembly as in ***Figure 4-2***).

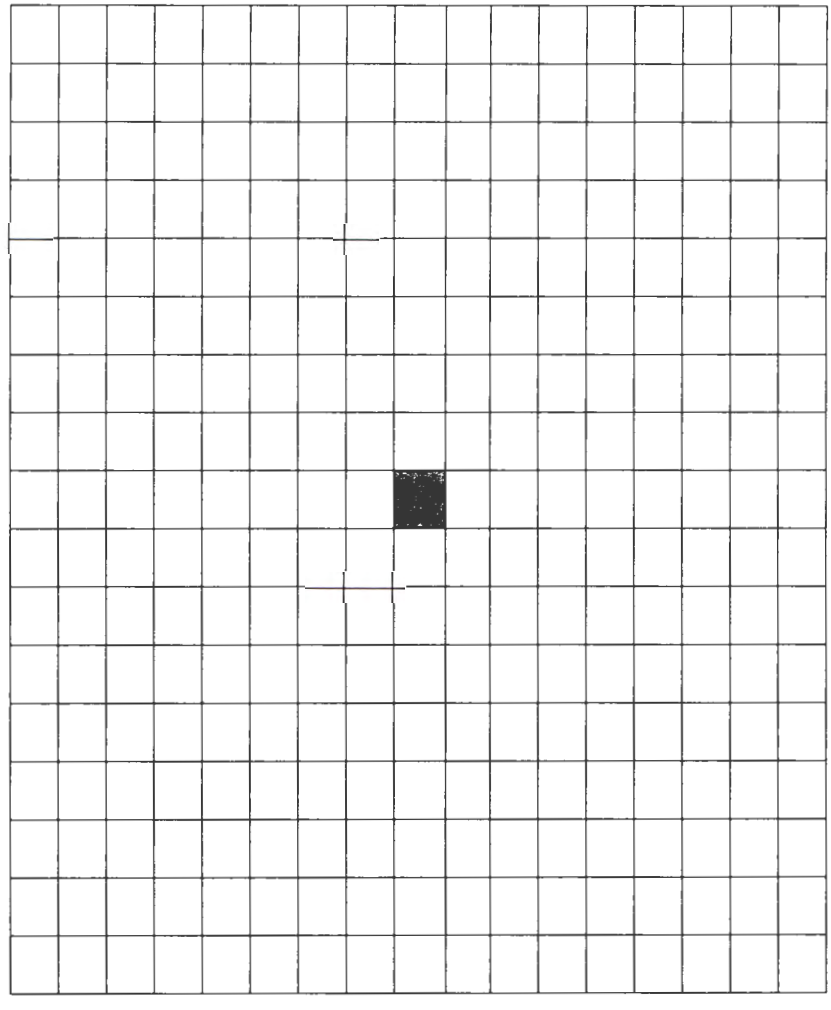

Figure 4-2: Flux Reconstruction Model of calculating reaction rates

However, it was also important to note that when the latter option was considered, flux reconstruction would have to be done for each assembly and this is usually expensive and time-consuming. It was decided to compare the results for both the above options to see which option yielded more accurate results as compared to plant data in order to decide on our final detector model. It could be expected that the latter option (flux reconstruction) would yield the best results, because this model takes into account all the heterogeneity in the assembly, but given the constraints mentioned above, maybe it wouldn't be a good idea to implement it in our final model of the detector. It would also be interesting to see

how the results obtained by calculating the averaged flux in the assembly would compare with plant data

4.3 Results from the comparison of plant detector values with those obtained from the MGRAC code

In this study, six cycles were selected from Koeberg Unit 2 reactor and core calculations for these cycles were performed using the MGRAC code. In order to get a representative picture over the total cycle history, eight detector maps from plant data were selected for each cycle and the MGRAC calculations were performed so that the some of the calculational steps correspond to cycle exposures of the flux maps. These eight maps were selected to represent the different burnup steps over the whole core burnup range but in some instances, this criterion could not be used effectively because there were insufficient plant data available at the exposures of interest. Since the core conditions in MGRAC were adjusted to be exactly the same as those under which the reference detector values (plant data) were obtained, it was therefore correct to compare the two directly. Due to the fact that not all assemblies were instrumented (i.e. had detectors inserted on them), it was also important to introduce a renormalization factor to the MGRAC detector responses so as to be able to compare the relative plant data map and the MGRAC values directly. For the eight detector maps, the maximum absolute percentage error and the root mean square percentage error (rms) for both the MGRAC detector map from average flux and reconstructed flux as compared to the measured reference detector values were calculated. The results obtained from this exercise are presented in ***Table 4-1***:

Table 4-1: Koeberg Unit 2 Cycle 1 Results

FLUX MAP NUMBER FOR PLANT DATA	BURNUP (MWD/te)	MAX. ABSOLUTE % ERROR		RMS % ERROR	
		NODE AVG. FLUX	RECONST. FLUX	NODE AVG. FLUX	RECONST. FLUX
20	1595.8	17.31	14.23	3.73	3.91
23	3901	15.09	12.57	3.07	3.27
34	5243.9	14.08	11.91	2.77	3.04
50	9498.1	16.14	16.25	7.59	7.82
56	10226.9	10.00	8.73	2.26	1.90
74	13011.9	8.86	7.74	2.20	1.72
77	13710	7.65	6.52	2.63	1.63
80	14438.9	7.21	5.37	2.82	1.60

Table 4-2: Koeberg Unit 2 Cycle 2 Results

FLUX MAP NUMBER FOR PLANT DATA	BURNUP (MWD/te)	MAX. ABSOLUTE % ERROR		RMS % ERROR	
		NODE AVG. FLUX	RECONST. FLUX	NODE AVG. FLUX	RECONST. FLUX
17	1698.4	5.48	4.67	2.55	2.11
19	3078.6	6.16	3.36	2.53	1.37
29	6253.1	8.03	4.97	3.09	1.52
37	8634	6.35	3.15	2.56	1.04
39	9381.6	9.27	5.67	4.29	3.70
42	10075.6	7.88	4.84	3.07	1.37
43	10271.1	7.84	4.94	3.08	1.33
45	10731.2	8.83	4.11	3.15	1.59

Table 4-3: Koeberg Unit 2 Cycle 3 Results

FLUX MAP NUMBER FOR PLANT DATA	BURNUP (MWD/te)	MAX. ABSOLUTE % ERROR		RMS % ERROR	
		NODE AVG. FLUX	RECONST. FLUX	NODE AVG. FLUX	RECONST. FLUX
5	235.3	8.83	12.24	4.77	6.09
15	590.7	8.19	11.09	4.27	5.54
19	2104.2	5.68	8.11	2.75	3.98
21	3750.5	4.24	6.68	1.93	2.87
31	6208.9	3.52	5.44	1.65	2.26
54	10822.9	4.00	4.21	1.49	1.83
56	11305.1	5.09	3.68	1.66	1.73
58	11650	4.64	4.05	1.48	1.81

Table 4-4: Koeberg Unit 2 Cycle 4 Results

FLUX MAP NUMBER FOR PLANT DATA	BURNUP (MWD/te)	MAX. ABSOLUTE % ERROR		RMS % ERROR	
		NODE AVG. FLUX	RECONST. FLUX	NODE AVG. FLUX	RECONST. FLUX
2	55.2	14.64	18.92	5.43	6.40
12	563.1	12.70	17.28	4.56	6.22
17	2241.8	10.5	14.96	3.23	4.55
32	4490.9	8.64	12.77	2.29	3.43
45	6322.5	6.82	10.73	2.22	2.74
48	7855.2	6.40	10.08	1.84	2.63
61	9177.2	6.52	9.02	2.42	1.90
63	10476.2	6.47	3.56	3.17	1.59

Table 4-5: Koeberg Unit 2 Cycle 5 Results

FLUX MAP NUMBER FOR PLANT DATA	BURNUP (MWD/te)	MAX. ABSOLUTE % ERROR		RMS % ERROR	
		NODE AVG. FLUX	RECONST. FLUX	NODE AVG. FLUX	RECONST. FLUX
3	69.7	11.69	14.23	5.53	5.99
15	665.3	10.20	14.03	4.11	5.45
25	1527.5	8.78	12.75	3.90	4.86
37	2462.8	7.81	11.73	3.05	4.15
41	4008	6.56	10.36	2.34	3.30
42	4615.4	5.74	9.51	2.10	3.10
57	7697.9	5.20	8.49	1.74	3.04
69	11508.7	7.35	3.91	3.70	2.03

Table 4-6: Koeberg Unit 2 Cycle 6 Results

FLUX MAP NUMBER FOR PLANT DATA	BURNUP (MWD/te)	MAX. ABSOLUTE % ERROR		RMS % ERROR	
		NODE AVG. FLUX	RECONST. FLUX	NODE AVG. FLUX	RECONST. FLUX
6	149.4	14.16	11.06	4.15	4.52
21	1896	11.52	8.00	3.23	3.07
23	3207.4	11.75	8.36	3.44	2.69
34	5745.3	7.65	5.36	2.67	1.96
49	8057.7	5.41	4.34	2.24	1.84
59	9972.8	5.31	3.73	2.67	1.43
61	10835.7	6.79	4.20	3.73	1.96
63	11552.3	6.88	4.30	3.91	2.10

4.4 Results from the comparison of plant detector values with those obtained from the MGRAC code and from a validated code, SCIENCE.

As a further evaluation of the detector model the predicted detector maps were also compared with results from another validated code. Since the reactor used for the validation of our detector model is Koeberg, it is therefore logical to compare our results (MGRAC) with results obtained from a validated code used at Koeberg namely, the SCIENCE code. The only data available to us for this purpose at the time when this study was done was for three cycles namely, cycles 4, 5, and 6. Again, this comparison was done, taking into consideration that not all assemblies had measurements taken from them, and hence it was necessary to introduce a renormalization factor to the SCIENCE values. As the situation is, the SCIENCE code actually relates the relative assembly power with detector reaction rates or plant data. In the same way, the RMS % error and the absolute maximum % error were calculated. The results for this exercise are therefore presented below: Note that in ***Table 4-7*** to ***Table 4-9*** below, a representative MGRAC detector value (using the node average flux) is compared to a corresponding MGRAC relative power value and the SCIENCE value for the relative power.

Table 4-7: Cycle 4 Results Comparison with Science Values

FLUX MAP # FOR PLANT DATA	BURNUP (MWD/te)	MAX. ABSOLUTE % ERROR			RMS % ERROR		
		REP. DET. VALUE	MGRAC REL. PWR.	SCIENCE	REP. DET. VALUE	REL. PWR.	SCIENCE
12	5631	12.70	31.00	32.00	9.69	6.22	10.86
47	7146	6.88	29.55	29.74	9.30	2.68	7.08
60	8850	5.87	28.45	20.2	9.27	2.26	5.80

Table 4-8: Cycle 5 Results Comparison with Science Values

FLUX MAP # FOR PLANT DATA	BURNUP (MWD/te)	MAX. ABSOLUTE % ERROR			RMS % ERROR		
		REP. DET. VALUE	REL. PWR	SCIENCE	REP. DET. VALUE	REL. PWR.	SCIENCE
14	411.7	10.63	35.35	26.31	4.66	10.29	16.97
39	3048.9	6.97	33.47	19.58	2.72	9.80	10.56
66	9350.9	4.96	29.90	16.04	1.65	10.69	6.72

Table 4-9: Cycle 6 Results Comparison with Science

FLUX MAP # FOR PLANT DATA	BURNUP (MWD/te)	MAX. ABSOLUTE % ERROR			RMS % ERROR		
		REP. DET. VALUE	REL. PWR.	SCIENCE	REP. DET. VALUE	REL. PWR.	SCIENCE
22	2512.6	10.41	33.30	17.08	2.95	8.71	9.25
36	6484.2	32.26	26.38	36.29	13.33	13.75	15.32
62	11489.2	9.25	27.74	11.80	4.08	8.74	5.10

The percentage differences between these sets of data are more pronounced when viewed through graphical representation and ***Figure 4-3*** below clearly depicts those differences:

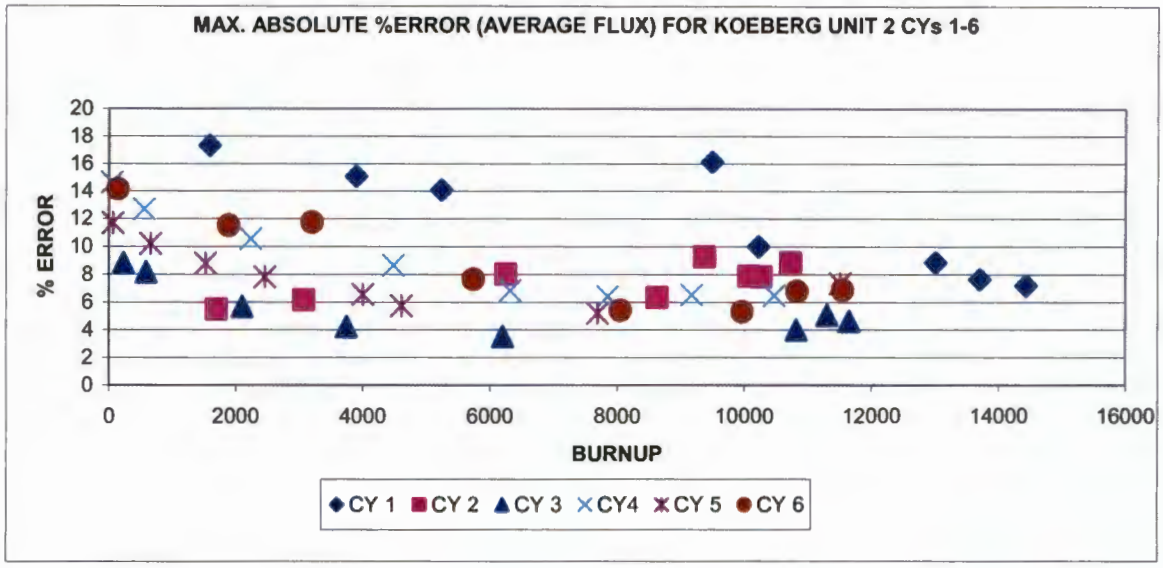

Figure 4-3: Max. absolute % error for the average flux at Koeberg 2 Cycles 1-6

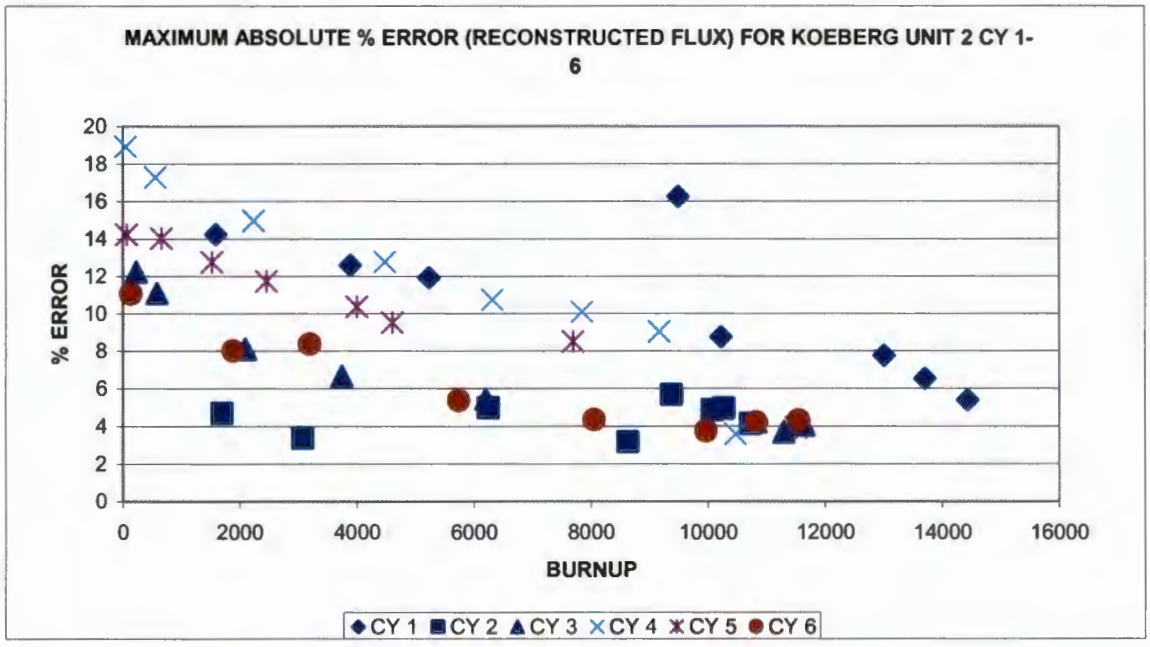

Figure 4-4: Max. absolute % error for reconstructed flux at Koeberg 2 Cycles 1-6

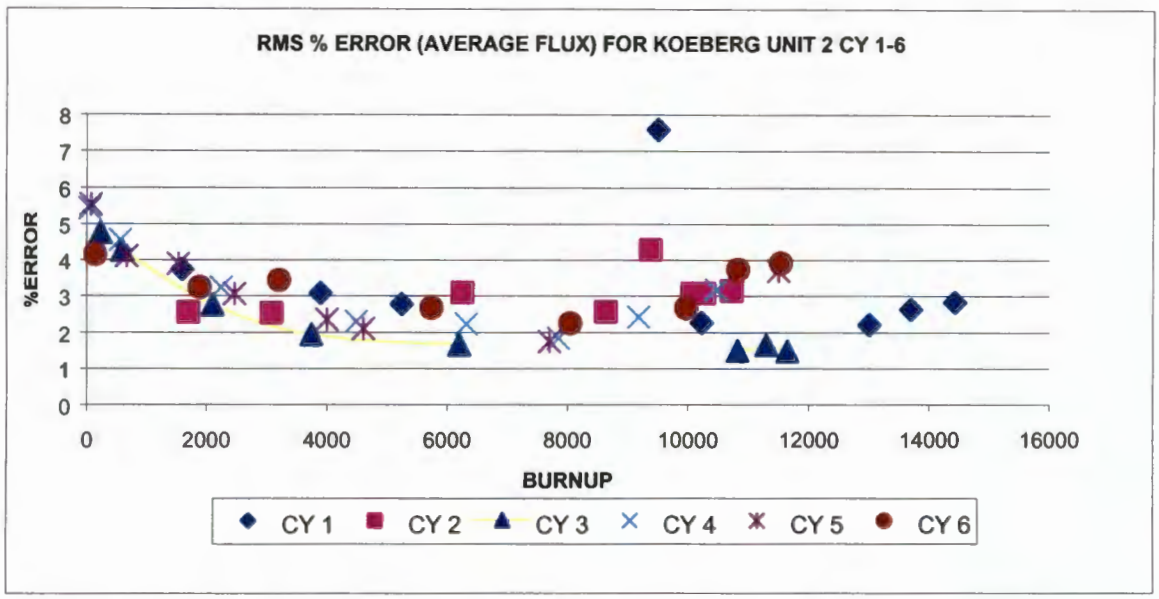

Figure 4-5:The root mean square % error for the average flux at Koeberg 2 Cycles 1-6

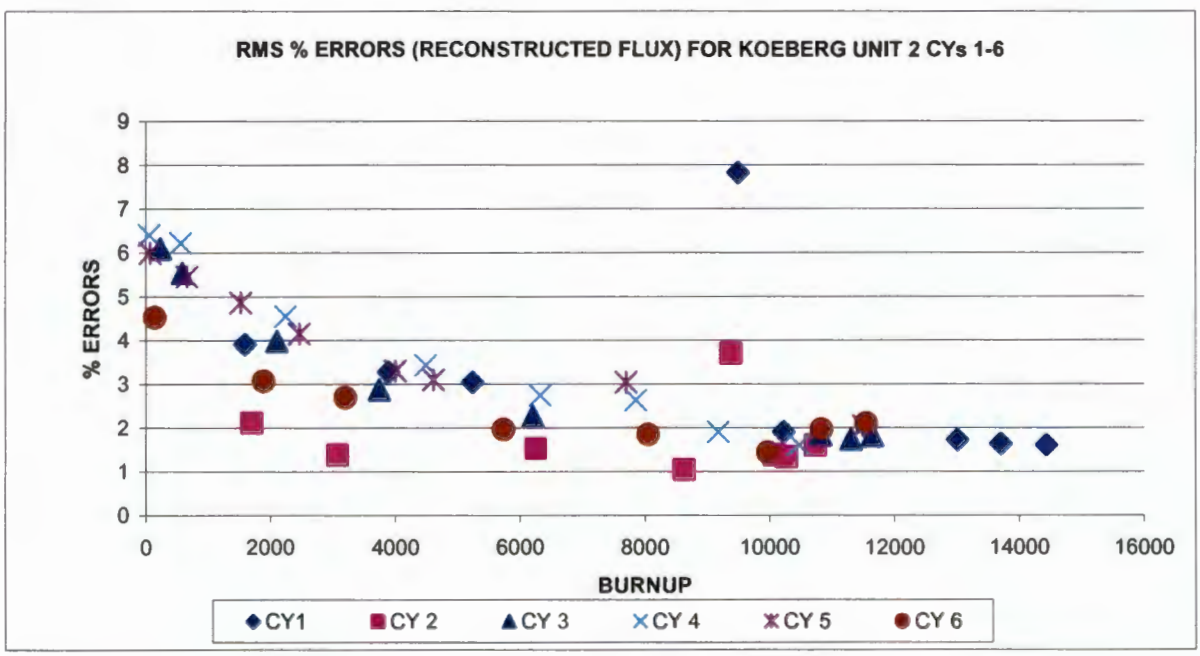

Figure 4-6:The root mean square % error (reconstructed flux) at Koeberg 2 Cycles 1-6

The above results and their implications to our final detector model will be discussed at length in the next section.

4.5 Discussion of the Results

In discussing the above results, it must first be noted that the whole exercise of performing the above calculations was aimed at evaluating the accuracy of the detector model that is being developed in this work before being used in the production version of the OSCAR 3 code system. It was also important to make sure that conditions under which the core calculations were performed were exactly the same as those under which plant data was obtained so as to make a fair comparison. Having ensured that all conditions were the same it was observed that the results obtained when using MGRAC yielded a fairly good approximation of the detector response relative to the plant data. The low RMS % errors yielded by MGRAC (of between 1 – 6%) calculations bears testimony to the fact that because of their more systematic and rigorous nature, the use of advanced nodal schemes in reactor core analysis provides accurate predictions of reactor conditions, hence the accuracy of our detector model. Except for some larger errors in the peripheral regions and a few large errors in the central regions of the core, the MGRAC results obtained in this study attests to the fact that the nodal methods have the capability of producing at least up to 2 % errors when used correctly (Lawrence, 1986).

However, it cannot be said at this stage as to which flux values from MGRAC are to be used in the final detector model because there is a fluctuation of the accuracy of the detector values for both the average and reconstructed flux from MGRAC. The RMS values shows an appreciably low error for MGRAC reconstructed flux in general for all the six cycles studied. However it is also observed that with the maximum absolute % error values, the reconstructed flux yields smaller errors for the first two cycles but this increase quite significantly in subsequent cycles whilst the error in the average flux decreases appreciably and this occurs mostly at the assemblies situated nearer to the core periphery, something we can expect due to the less burnt fuel in these regions.

The extent of uranium enrichment of the fuel in these cycles may also be the reason why we notice this trend. In the graphs shown above, (***Figure 4-3*** to

Figure 4-6) the shape of the graphs is also as expected because as burnup increases we expect the error to decrease. The error "burn away" as areas with too high flux will burn away more and hence a self-levelling effect will occur. Exceptions to this trend were found for several points in cycle 1 and 2 where we observe a sharp increase of the % error around 9000 MWD/te. This may perhaps be attributed to power renormalization problems, boron concentration uncertainties and control rods movement.

An important observation must also be noted that when comparing plant data with SCIENCE and our MGRAC relative power results, generally the errors are too large. Neither MGRAC nor SCIENCE yields a better prediction of the plant data. The reason for this we believe is that the philosophy of using relative power densities and adjusting them with the help of measured detector values (as used in SCIENCE) is not a good idea. We propose that the better way is to predict the actual detector response and use that for comparisons and adjustments, and hence there is an inevitable need to have a detector model in the code in order to depict the true detector response.

CHAPTER 5 DISCUSSIONS, CONCLUSIONS AND RECOMMENDATIONS FOR FUTURE WORK

5.1 Discussions

This work was aimed at developing a neutron detector model to be used in nodal diffusion codes and was therefore incorporated into the OSCAR-3 code system, in order to verify the efficiency of such a detector model through validation of this code. The development of this neutron detector model took into consideration various theoretical arguments that would warrant its use for the validation of OSCAR-3 in any PWR reactor with similar incore neutron detectors These arguments encapsulate *inter alia*, how the detector constant (fission cross section of ^{235}U) respond to certain changes in the core parameters like the boron concentration, fuel temperature, moderator temperature and density and these have been found to behave exactly as theoretically expected. The influences of both the one group and the two-group detector constant on our final detector model have also been examined.

From the sensitivity studies carried out, the following inferences can be drawn:

- The one group detector constants are sensitive to :
  - Assembly type and burnup.
  - Core conditions like moderator temperature and boron concentration.
  - Fuel temperature but to a lesser extent (i.e. less sensitive to this variation).
- The two group detector constants (fast and thermal) are less sensitive to these changes.

Although it would have been good to have the detector model evaluated both cases, it can conveniently be said that the two group detector constant model are supposed to be more accurate than the one-group because the one group is more sensitive and would yield

worse results. This gives a strong indication of the robust nature of the methods, and the overall calculational accuracies of the neutronics workhorse of the OSCAR 3 code system, MGRAC. It is also important to note that the detector model provide an additional tool to perform the validation of the code. This, however, does not form the scope of this work.

Unfortunately, due to insufficient data, it has been difficult and to some extent, impossible to establish the effectiveness and the validity of our detector model in other cycles at Koeberg beyond cycle 6. This is particularly important to point out since more advanced assembly designs with different fuel enrichment and Gd loading are being introduced from cycle 8 and beyond and it could have been also interesting to see how the detector model performed under these conditions. Also, in spite of the fact that there is generally (on average), less % errors relative to plant data in our results using MGRAC, it is also a general observation that these large errors occur mostly in the assemblies that are situated in the core periphery as seen in ***Appendix E***. This could be expected since steep flux shapes are found in the peripheral zones due to neutron leakage into the reflector.

5.2 Conclusions

This work has at the most achieved what it sought to achieve, i.e. to develop a fission detector model and to evaluate it against plant data. This detector model has been established and its behaviour is well understood. The implementation of this model into the OSCAR-3 system yields good results. The author further recommends that the detector model developed in this work be introduced into the production version of the OSCAR-3 code system and consequently be used to perform the production runs of the Koeberg Nuclear Power Station.

5.3 Recommendations for future work

A number of things have not been done to bring this work to its logical conclusion although that does not affect the conclusions drawn above. First, it would be desirable, as stated above, to see the results that MGRAC would yield, using a one-group detector constant especially if any dependence on exposure and core conditions is ignored. It is recommended that this part be pursued for the sake of fairly judging the efficiency of MGRAC as against the SCIENCE code, which has already been validated for Koeberg, thereby allowing the custodians of the OSCAR-3 code to have a full picture of the performance of this code for the Koeberg reactors. This can also assist in the marketing of the OSCAR-3 code for PWRs in general. Secondly, the validation of the detector model for the new fuel assemblies that have recently been introduced at Koeberg is required to ensure its applicability for all fuel types in any PWR.

APPENDIX A: ASSEMBLY SPECIFICATIONS

All physical dimensions given here are at cold conditions (i.e. 20 °C).

FUEL PIN:

Fuel pellet radius	0.40950 cm
Zircalloy-4 clad inner radius	0.41775 cm
Zircalloy-4 clad outer radius	0.47475 cm

GUIDE TUBE AND INSTRUMENTATION THIMBLE:

Tube inner radius (Zircalloy-4)	0.570 cm
Tube outer radius (Zircalloy-4)	0.612 cm

CONTROL ROD:

Absorber radius (Ag-In-Cd)	0.433 cm
Clad inner radius (SS-304)	0.437 cm
Clad outer radius (SS-304)	0.484 cm

BURNABLE ABSORBER ROD:

(Pressurised with helium)

Inner radius of inner clad (SS-304)	0.2210 cm
Outer radius of inner clad (SS-304)	0.2375 cm
Inner radius of BA (Boron-silicate glass)	0.2415 cm
Outer radius of BA (Boro-silicate glass)	0.4265 cm
Inner radius of outer clad (SS-304)	0.4370 cm
Outer radius of outer clad (SS-304)	0.4840 cm

GENERAL ASSEMBLY SPECIFICATIONS:

Reactor lattice	17 x 17
Fuel pin pitch	1.26 cm
Fuel assembly pitch (including water gap)	21.504 cm
Fuel rods per assembly	264
Number of guide tubes for control rods	24
Number of instrumentation tubes	1
Active assembly height	365.76 cm
Total height of cluster	385.15 cm
Mass of grids in active length	4275.975 g
Mass of sleeves in active length	821.0 g

FUEL COMPOSITIONS:

Mass UO_2 per fuel pin (1.8, 2.4, 3.1 and 3.25 wt%)	2006 g
Mass UO_2 per fuel pin (3.9 wt%)	1974 g
Mass UO_2 per fuel pin (3.9 wt% with 8 wt% Gd_2O_3)	1816 g

MATERIAL CHARACTERISTICS:

Material	Density (g/cm^3)
UO_2 (95% of theoretical density)	10.412
Zircalloy-4	6.55
Coolant	1.00
Inconel 718	8.20
Ag-In-Cd control	10.16
Stainless steel 304	7.90
Helium	0.0001
Boro-silicate	2.237

APPENDIX B: REFLECTOR SPECIFICATIONS

All physical dimensions given here at hot operating conditions

BAFFLE:

Thickness	2.8575 cm
Material	SS-304
Density	7.93 g/cm^3
Composition	Co - 0.12 wt%
Ni - 10.00 wt%	
Cr - 18.00 wt%	
Fe - 71.88 wt%	

REFLECTOR

Thickness	18.7505 cm
Material	H_2O + soluble boric acid
Density	0.753994 g/cm^3 (corresponding to inlet water temperature of 286 °C)

APPENDIX C: PARAMETERS USED IN FUEL ASSEMBLY CALCULATIONS

Expanded fuel pin pitch 1.265197 cm

Expanded fuel assembly pitch (including water gap) 21.612349 cm

Table C.1: Number Densities for Uo_2 Fuel

Isotope	U^{235} enrichment				
	1.8	**2.4**	**3.1**	**3.25**	**3.9**
U-234	-	-	-	-	8.9402E-06
U^{235}	4.1810E-04	5.5746E-04	7.2004E-04	7.5488E-04	8.9048E-04
U-236	-	-	-	-	4.5458E-06
U-238	2.2521E-02	2.2384E-02	2.2223E-02	2.2188E-02	2.1652E-02

Table C.2: Number Densities for Uo_2 Fuel With Gadolinium

Isotope	U^{235} enrichment
	0.4
U-234	8.2254E-06
U^{235}	8.4029E-05
U-236	4.1823E-06
U-238	2.0647E-02
Gd-152	5.3727E-06
Gd-154	5.9100E-05
Gd-155	4.0027E-04
Gd-156	5.5339E-04
Gd-157	4.2176E-04
Gd-158	6.6353E-04
Gd-160	5.8294E-04

Table C.3: Fuel Pin Specifications (Expanded)

Radius (cm)	0.412227	0.475675	0.713811
Material	Fuel	Cladding	Water + structure
Temperature (K)	951.358	609.563	579.442
Number densities			
Zr		3.9004E-02	
H			4.7414E-02
O			2.3707E-02
B-10			4.6927E-06
Fe (WIMS mat 56)			6.0170E-05
Fe (WIMS mat 1056)			2.5787E-05
Ni			2.9823E-04
Cr			1.1404E-04

Table C.4: Guide Tube Specifications (Expanded)

Radius (cm)	0.570955	0.613025	0.713811
Material	Water	Zircalloy + Structure	Water + Structure
Temperature (K)	579.442	579.442	579.442
Number Densities			
H	4.7689E-02		4.7414E-02
O	2.3844E-02		2.3707E-02
B-10	4.7200E-06		4.6927E-06
Fe (WIMS mat 56)		3.1342E-03	6.0170E-05
Fe (WIMS mat 1056)		1.3432E-03	2.5787E-05
Ni		5.6595E-04	2.9823E-04
Cr		1.2779E-03	1.1404E-04
Zr		4.3092E-02	

Note: The outermost radius is the radius of a cylinderized cell corresponding to a pin pitch of 1.265197 cm.

Table C.5: Burnable Absorber Rod Specifications Expanded)

Radius (cm)	0.222120	0.241722	0.426892	0.486453
Material	Helium	SS-304	Boro-silicate glass	SS-304
Temperature (K)	579.442	579.442	579.442	579.442
Number densities				
He	1.4820E-05			
B-10			9.5424E-04	
O			4.9247E-02	
Na			1.6474E-03	
Si			1.8803E-02	
Fe (WIMS mat 56)		3.5746E-02		3.4185E-02
Fe (WIMS mat 1056)		1.5320E-02		1.4651E-02
Ni		6.4547E-03		6.1728E-03
Cr		1.4575E-02		1.3938E-02

Note: Burnable absorber rods are inserted inside the guide tube.

Table C.6: Control Rod Specifications (Expanded)

Radius (cm)	0.435789	0.486453
Material	Ag-In-Cd	SS-304
Temperature (K)	579.442	579.442
Number densities		
Ag-In-Cd	1.0000E+00	
Fe (WIMS mat 56)		3.9801E-02
Fe (WIMS mat 1056)		1.7058E-02
Ni		7.1869E-03
Cr		1.6228E-02

Note 1: Control rods are inserted inside the guide tube (***Table C.4***).

Note 2: The control rod material (Ag-In-Cd) is represented by macroscopic cross sections prepared for a typical control rod at 600 K and inserted originally in the WIMS library.

APPENDIX D: BURNABLE POISON LOADING AT THE KOEBERG REACTORS

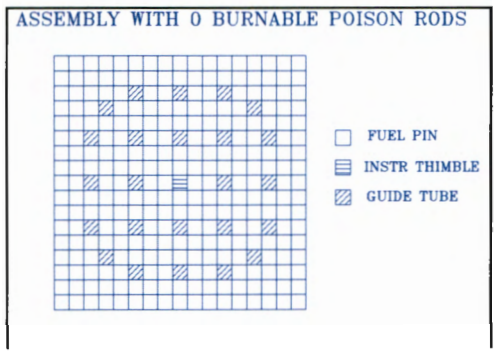

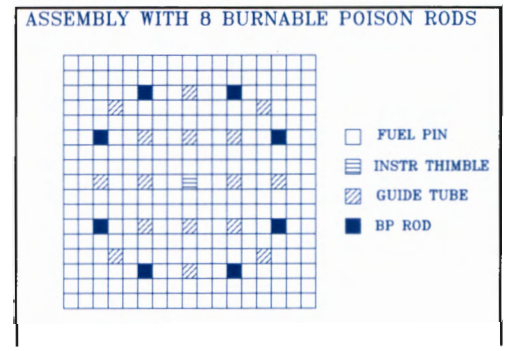

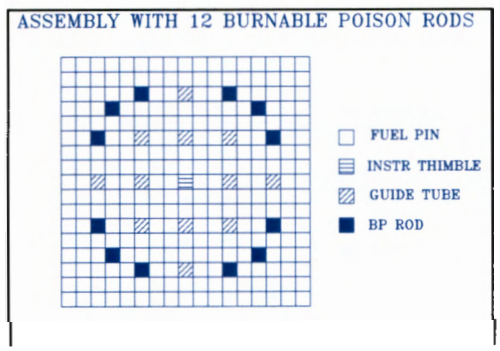

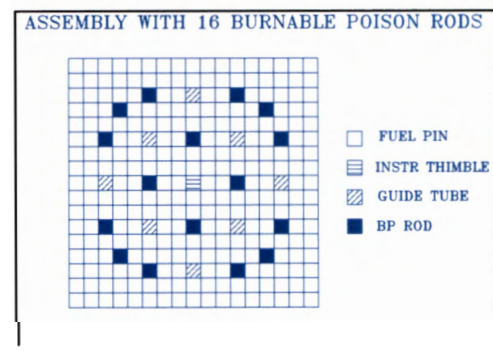

REFERENCES

1. **Askew J.R.** [1972]

   "Some Boundary Condition Problems Arising in the Application of Collision Probability Methods" Report AEEW-M 1094, Atomic Energy Establishment, Winfrith, UK (1972)

2. **Bell G.I., Glasstone S.** [1970]

   Nuclear Reactor Theory, Van Nostrand Reinhold Co, New York

3. **Carlvik, I** [1967]

   "Integral Transport Theory in One-Dimension Geometries", Nukleonik, 10, p 104

4. **Duderstadt J.J. Hamilton L.J.** [1976]

   Nuclear Reactor Analysis, John Wiley & Sons, New York

5. **Glasstone S, Sensonske A** [1981]

   Nuclear Reactor Engineering, 2nd edition, Van Norstrand Reinhold Co. New York

6. **Hoxie C.L., Henry A.F.** [1981]

   "Reconstruction of Heterogeneous PWR Flux Shapes from Nodal Calculations," Trans. Am. Nucl. Soc., *39*, p 905, December 1981

7. **Joanou G.D. Triplett J.R., Wagner R.M.** [1964]

   "An eigenvalue Method for the Calculation of Nuclear Burnup" Nucl. Sci. and Eng., 18, p.363 (1964)

8. **Joubert W.R.**[1992]

   "HEADE: A Two Dimensional Transport Theory Code for Heterogeneous Assembly Depletion Calculations. User's Manual", Report PIN 1367, Atomic Energy Corporation of South Africa.

9. **Khalil H.S.** [1983]

"The Application of Nodal Methods to PWR Analysis", Ph.D. thesis, Department of Nuclear Engineering, Massachusetts Institute of Technology.

10. **Khalil H.S. Hoxie C.L., Finck P.J., Parsons D.K., Henry A.F.** [1989]

"The Application of Nodal Methods to Light Water Reactors", Proceedings of the ANS Topical Meeting on "Advances in Reactor Physics and Core Thermal Hydraulics" Vol. 1, p. 348, Kiamesha Lake, New York September 1989

11. **Koebke K, Wagner M.R.** [1977]

"The Determination of the Pin Power Distribution in a Reactor Core on the Basis of Nodal Coarse Mesh Calculations", Atomkernenergie (ATKE), Bd. 30 Lfg. 2, p. 136, 1977

12. **Koebke K, Wagner M.R.** [1983]

"Progress in Nodal Reactor Analysis", Atomkernenegie-Kerntechnik, vol 43, no 2 (1983) p. 177

13. **Lawrence R.D.** [1986]

Progress in Nodal Methods for the Solution of the Neutron Diffusion and Transport Equations," Prog. Nucl. Energy, 17, p. 271

14. **Macfarlane R.E.** [1993]

NJOY91.91: A Code System for Producing Pointwise and Multigroup Neutron and Photon Cross Sections from ENDF/B Evaluated Nuclear Data" Report PSR-171, Oak Ridge National Laboratory (1983)

15. **Muller E.Z.** [1989]

"Development of an Environment-Insensitive PWR Radial Reflector Model Applicable tp Modern Nodal Reflector Analysis Methods", Ph.D. Thesis, Potchefstroom University for CHE, South Africa

16. **Muller E.Z., Ball G, Joubert W.R., Schutte H.C., Stoker C.C, Reitsma F,** [1994]

"Development of a Core Follow Calculational System for Research Reactors" 9th Pacific Basin Nuclear Conference, Sydney, Australia, 1-6 May 1994

17. **Reitsma, F. Joubert W.R.**[2000]

Koeblib 3.0: A Two Dimensional Polynomial Cross Section Library for Koeberg in Two, Four and Six Energy Groups, Report PIN 331, Atomic Energy Corporation of South Africa

18. **Reitsma, F.** [1998]

"The Application of Advanced Homogenization Models to the Reflector Regions of Boiling Water Reactors", MSc Thesis, Department of Physics, Potchefstroom University for Christian Higher Education, 1998

19. **Rose P.F., Dunford C.L** [1990]

ENDF-102: Data Formats and Procedures for the Evaluated Nuclear Data File, ENDF-6", Report BNL-NCS-44945, Brookhaven National Laboratory

20. **Smith K.S.** [1980]

"Spatial Homogenization Methods for Light Water Reactor Analysis," Ph.D. Thesis, Department of Nuclear Engineering, MIT, Cambridge, Massachusetts, USA

21. **Smith K.S.** [1986]

"Assembly Homogenization Techniques for Light Water Reactor Analysis", Prog. Nucl. Energy, 17, p.303

22. **Smith K.S.** [1991]

"Modern Reactor Core Design Codes and Comparison to Measured Data, Prog. Nucl. Energy, 22, p.105

23. **Taubman C.J.** [1975]

The WIMS 69-Group Library Tape 166259," Report AEEW-M-1324, Atomic Energy Establishment, Winfrith, UK

24. **Tong L.S. Weisman J.** [1979]

Thermal Analysis of Pressurized Water Reactors, 2nd Edition, ANS, LaGrange Park, 1979

Results 1: KOEBERG UNIT 2 CYCLE 4 TIP MEASUREMENTS
Results 2: UNIT 2: KOEBERG Cycle 4 3-D calc

Case 8 : MAP 12: DEPLETION-86%--POW = 100%
Layer 1

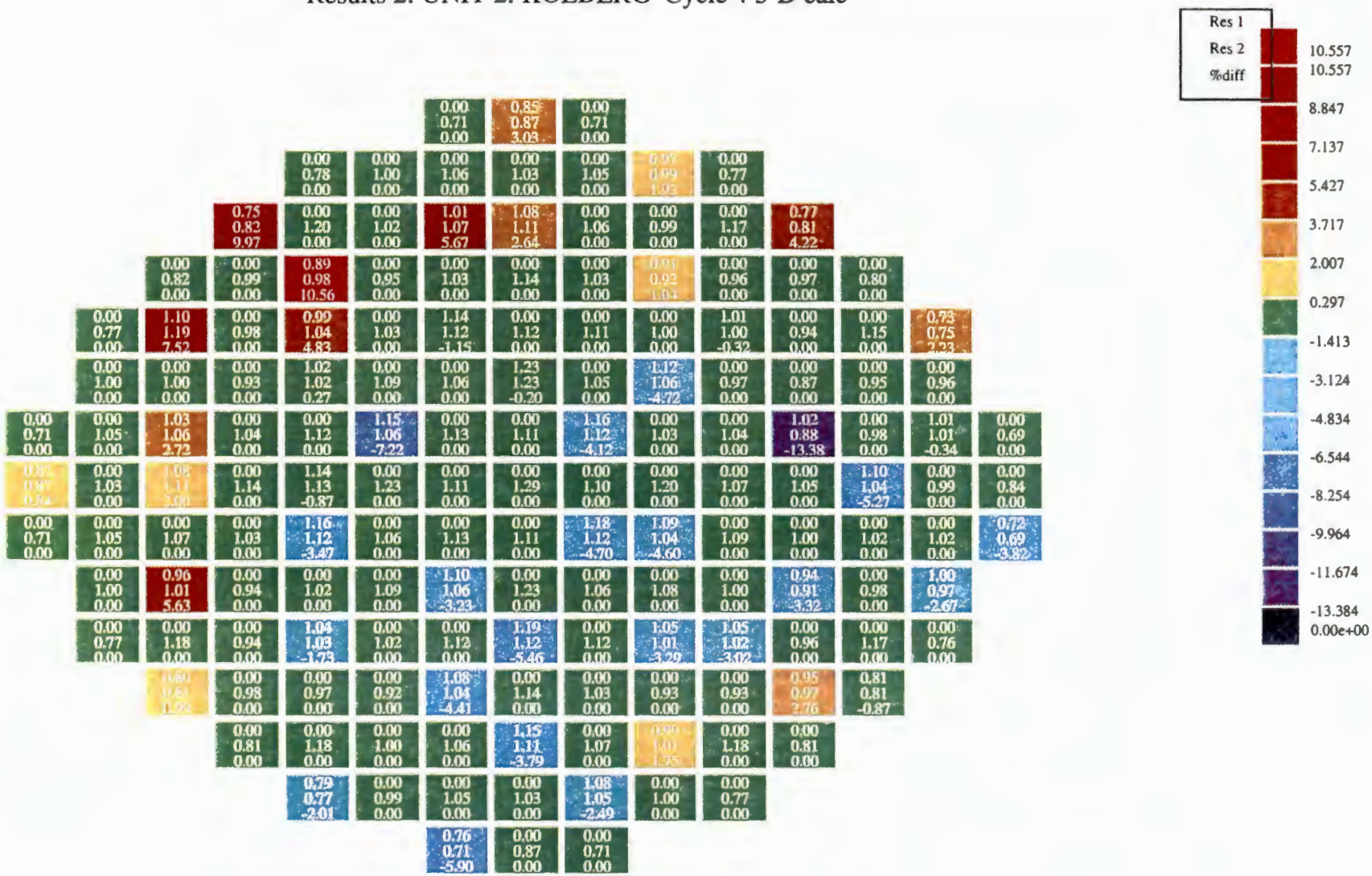

Differences between calculated and measured detector responses for Koeberg 2 Cycle 4 Map 12 : Nodal Average Flux applied

Detector Response - Average Flux

Colour: %diff

Results 1: KOEBERG UNIT 2 CYCLE 4 TIP MEASUREMENTS
Results 2: UNIT 2: KOEBERG Cycle 4 3-D calc

Case 8 : MAP 12: DEPLETION-86%--POW = 100%
Layer 1

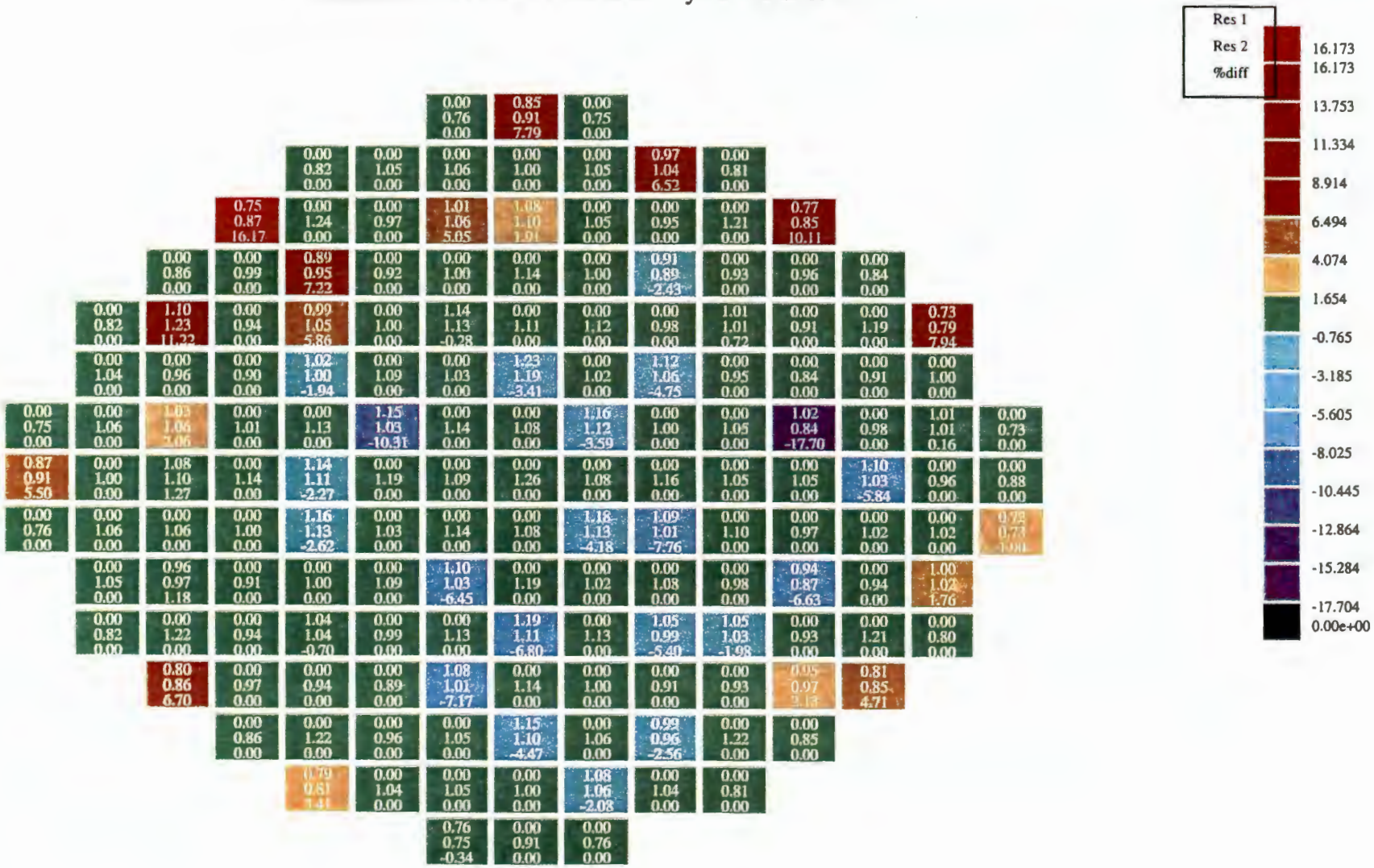

Differences between calculated and measured detector responses for Koeberg 2 Cycle 4 Map 12 : Reconstructed flux applied

Detector Response - Reconstructed Flux

Colour: %diff

Results 1: KOEBERG UNIT 2 CYCLE 4 TIP MEASUREMENTS
Results 2: UNIT 2: KOEBERG Cycle 4 3-D calc

Case 23 : MAP 48: DEPLETION---POW = 100%
Layer 1

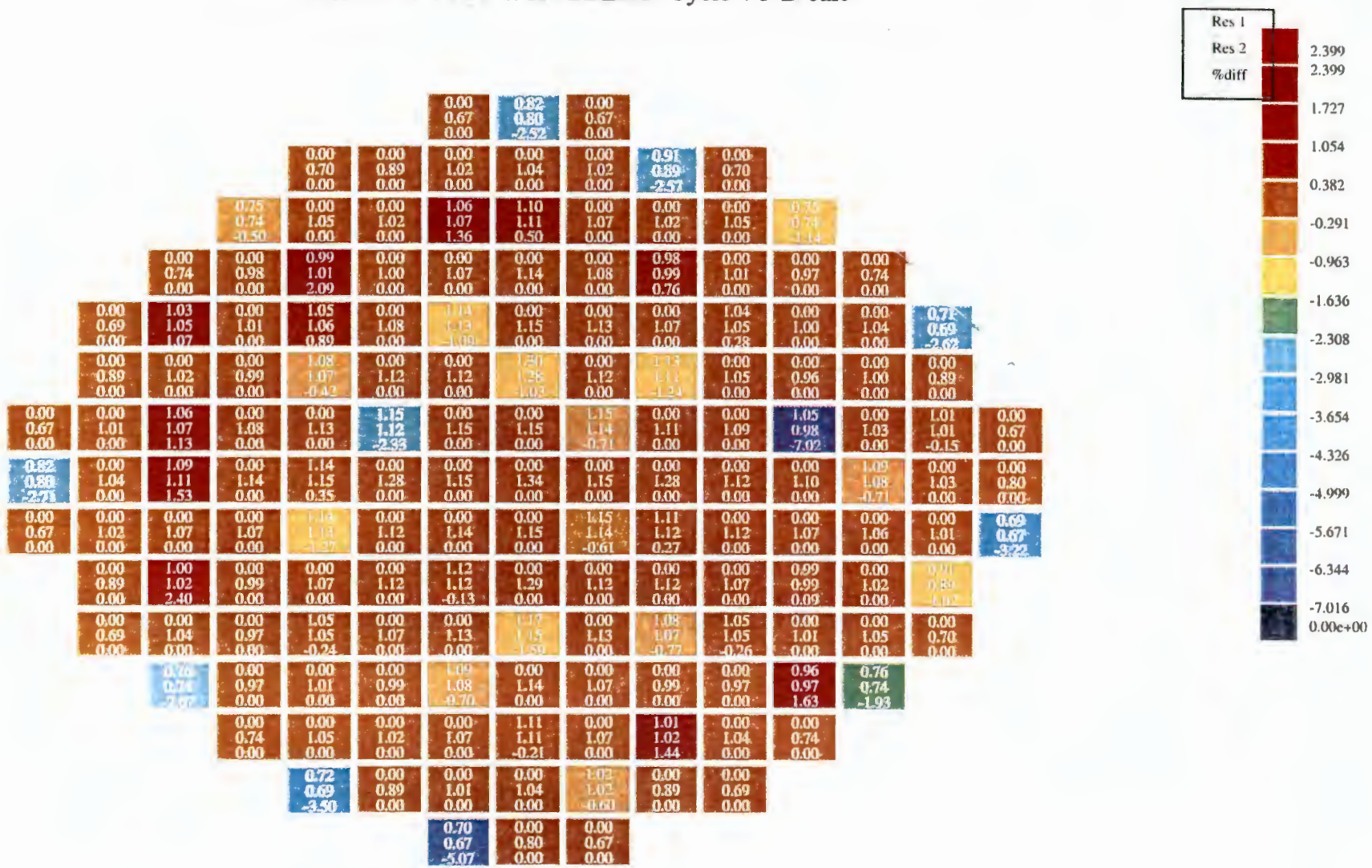

Differences between calculated and measured detector responses for Koeberg 2 Cycle 4 Map 48 : Nodal Average Flux applied

Detector Response - Average Flux

Colour: %diff

Results 1: KOEBERG UNIT 2 CYCLE 4 TIP MEASUREMENTS
Results 2: UNIT 2: KOEBERG Cycle 4 3-D calc

Case 26 : MAP 61: DEPLETION---POW = 94%, no boron
Layer 1

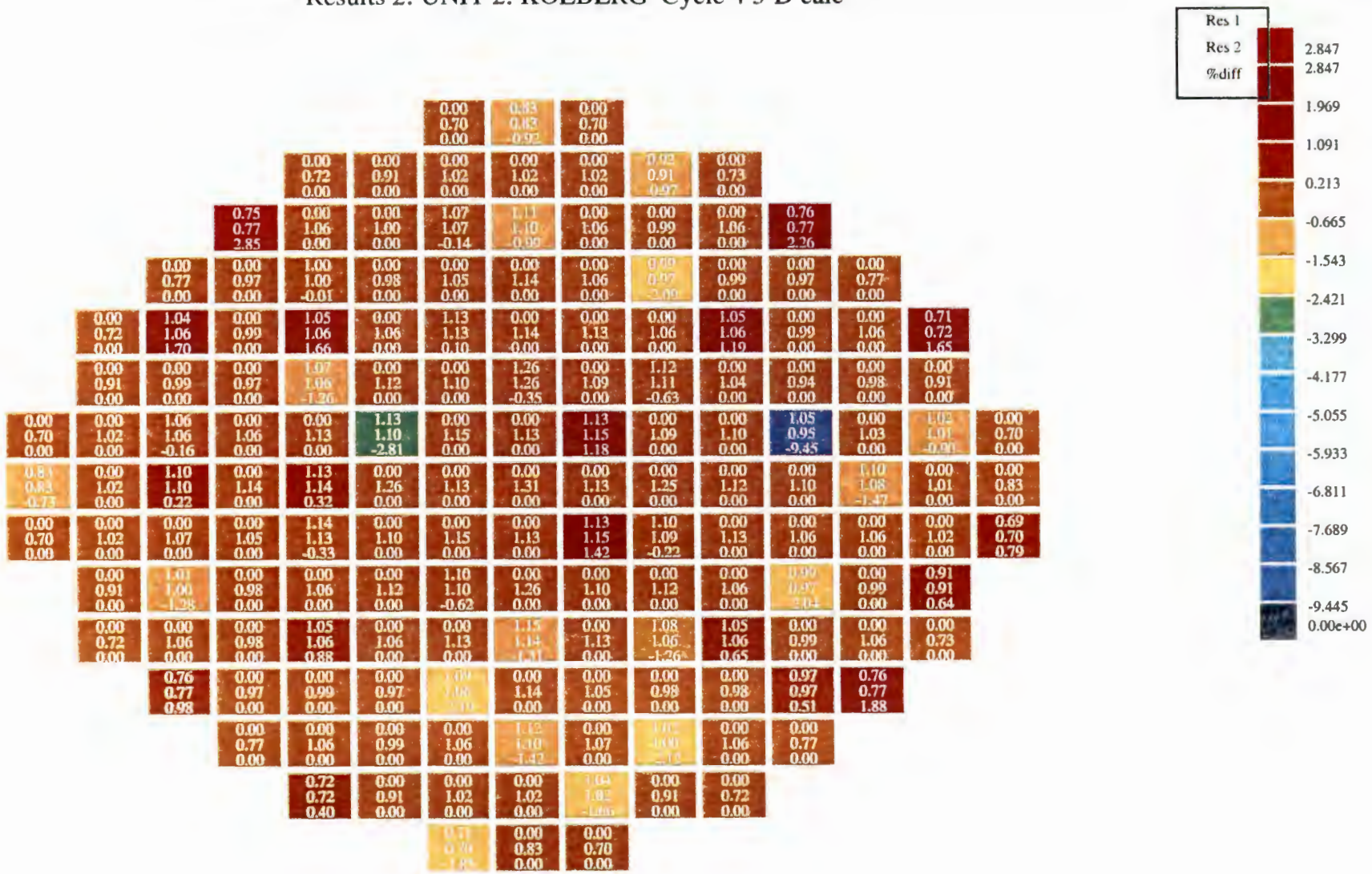

Differences between calculated and measured detector responses for Koeberg 2 Cycle 4 Map 61 : Reconstructed Flux applied

Detector Response - Reconstructed Flux

Colour: %diff

Results 1: KOEBERG UNIT 2 CYCLE 5 TIP MEASUREMENTS
Results 2: UNIT 2: KOEBERG Cycle 5 3-D calc

Case 11 : MAP 15: DEPLETION---POW = 100%
Layer 1

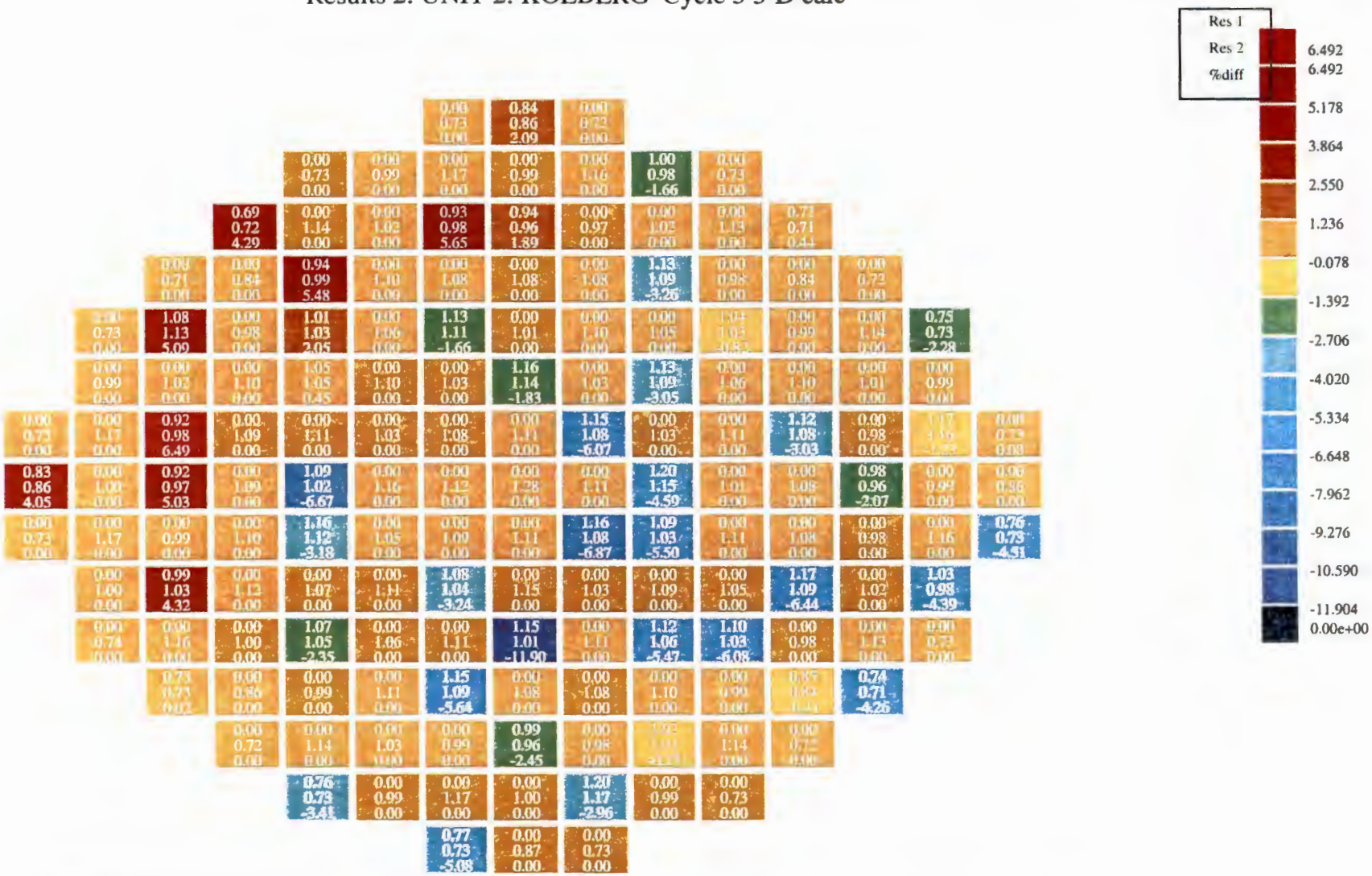

Differences between calculated and measured detector responses for Koeberg 2 Cycle 5 Map 15 : Nodal average Flux applied

Detector Response - Average Flux

Colour: %diff

Results 1: KOEBERG UNIT 2 CYCLE 5 TIP MEASUREMENTS
Results 2: UNIT 2: KOEBERG Cycle 5 3-D calc

Case 21 : MAP 41: DEPLETION---POW = 63%
Layer 1

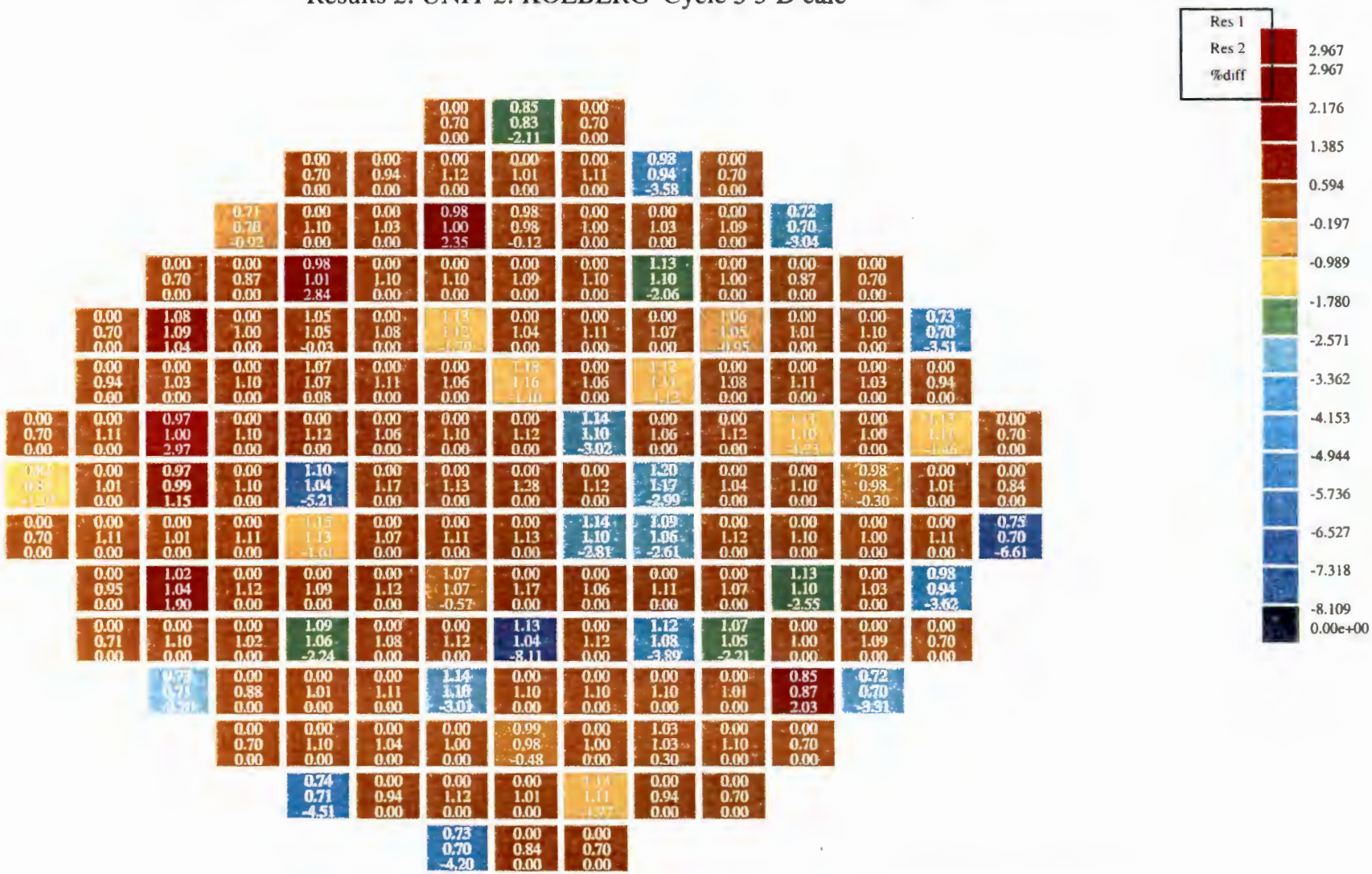

Differences between calculated and measured detector responses for Koeberg 2 Cycle 5 Map 41 : Nodal average Flux applied

Detector Response - Average Flux

Colour: %diff

Results 1: KOEBERG UNIT 2 CYCLE 5 TIP MEASUREMENTS
Results 2: UNIT 2: KOEBERG Cycle 5 3-D calc

Case 33 : MAP 69: DEPLETION---POW = 52%
Layer 1

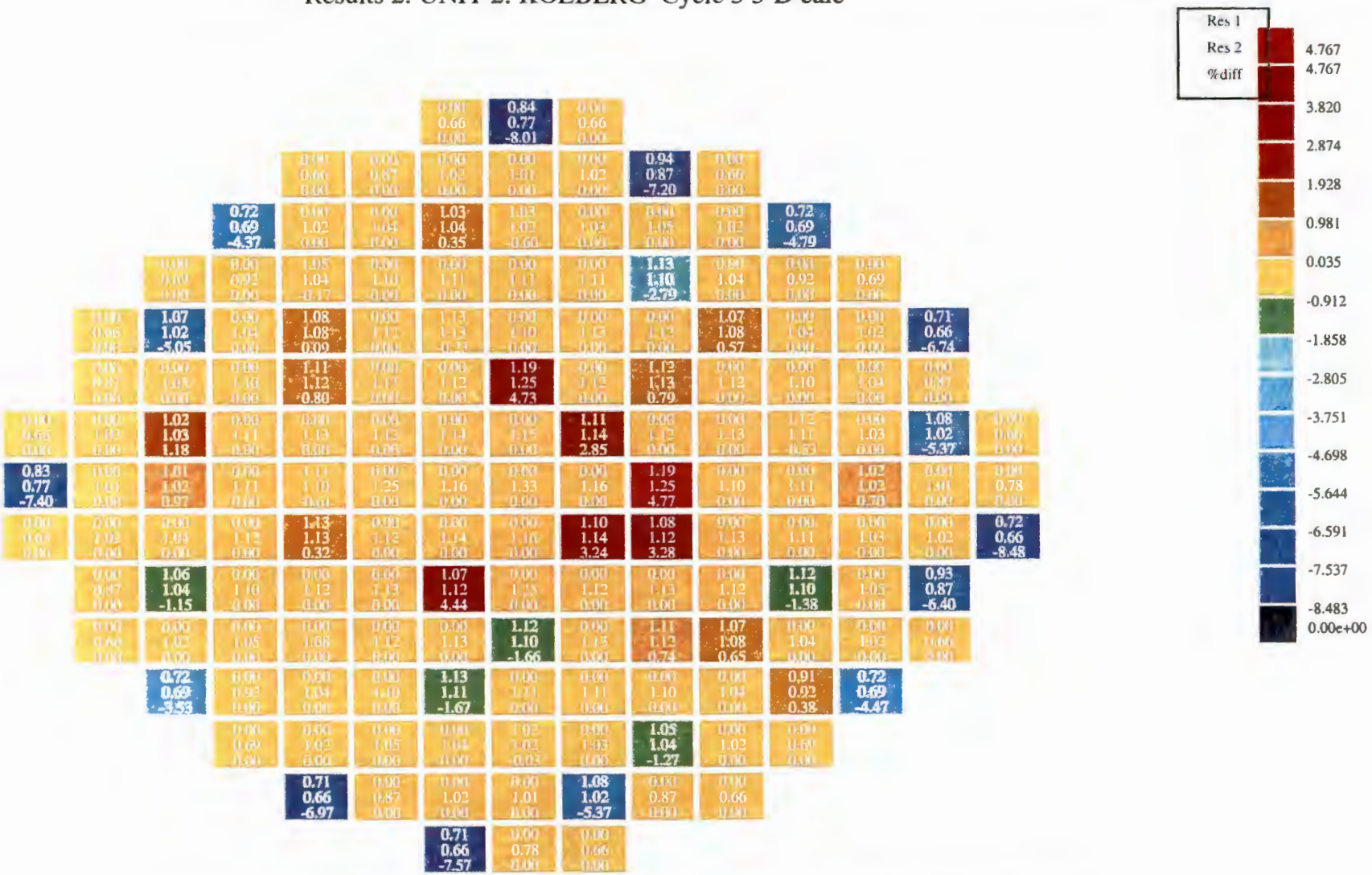

Differences between calculated and measured detector responses for Koeberg 2 Cycle 5 Map 69: Nodal Average Flux applied

Detector Response - Average Flux

Colour: %diff

Results 1: KOEBERG UNIT 2 CYCLE 6 TIP MEASUREMENTS
Results 2: UNIT 2: KOEBERG Cycle 6 3-D calc

Case 8 : MAP 21: DEPLETION---POW = 100%
Layer 1

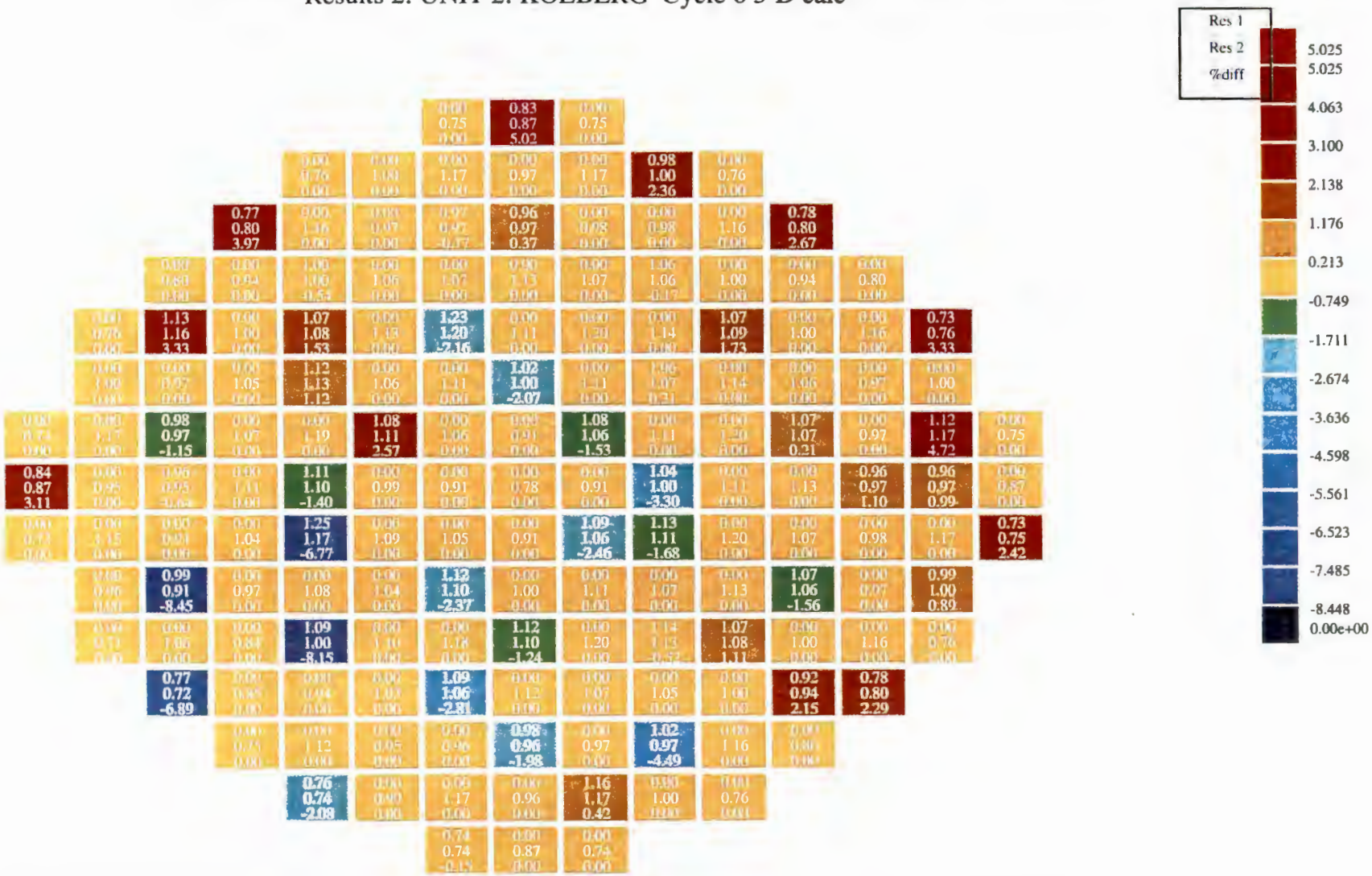

Differences between calculated and measured detector responses for Koeberg 2 Cycle 6 Map 21 : Reconstructed Flux applied

Detector Response - Reconstructed Flux

Colour: %diff

Results 1: KOEBERG UNIT 2 CYCLE 6 TIP MEASUREMENTS
Results 2: UNIT 2: KOEBERG Cycle 6 3-D calc

Case 14 : MAP 34: DEPLETION---POW = 63%
Layer 1

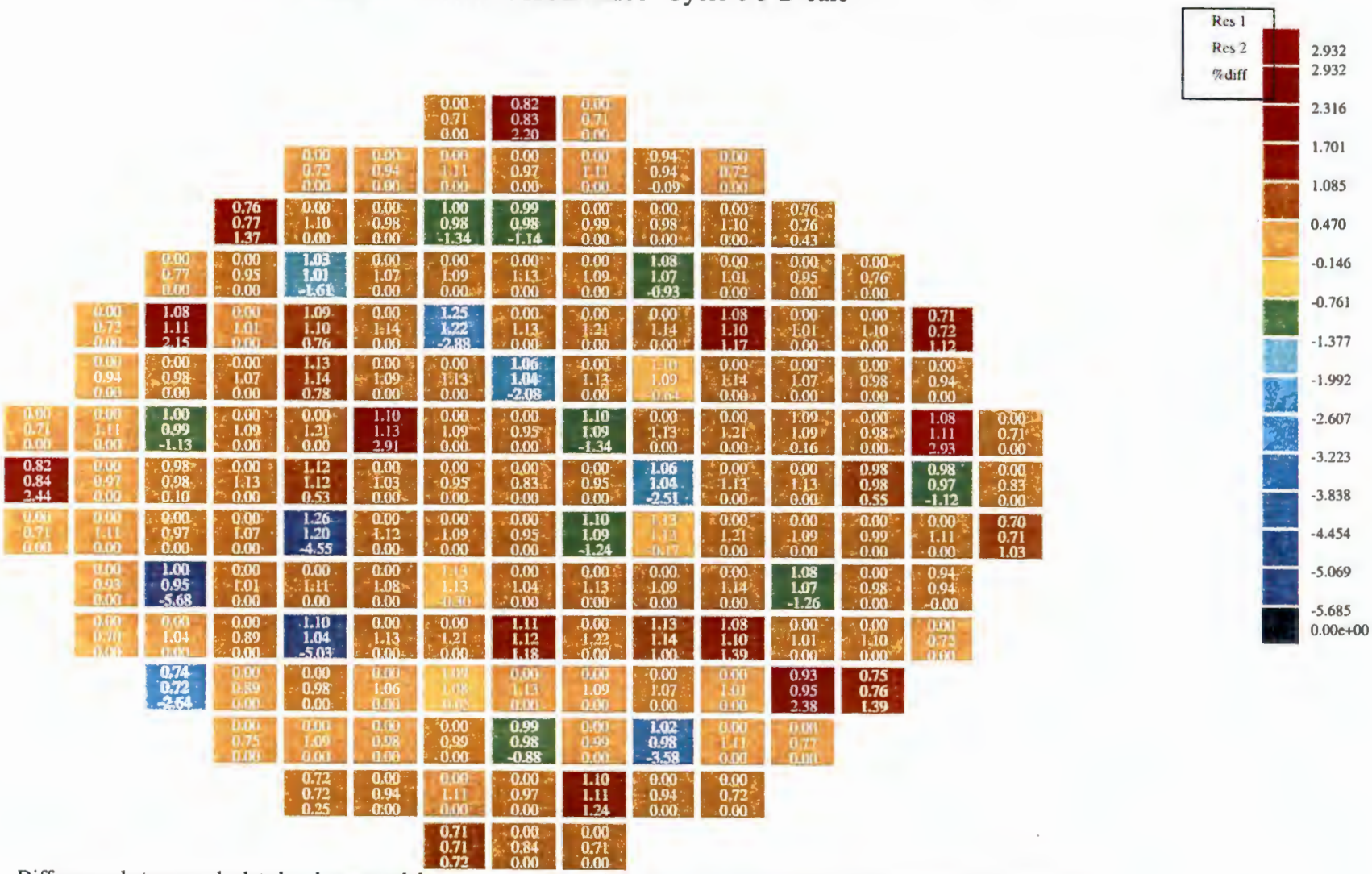

Differences between calculated and measured detector responses for Koeberg 2 Cycle 6 Map 34 : Reconstructed Flux applied

Detector Response - Reconstructed Flux

Colour: %diff

Results 1: KOEBERG UNIT 2 CYCLE 6 TIP MEASUREMENTS
Results 2: UNIT 2: KOEBERG Cycle 6 3-D calc

Case 8 : MAP 21: DEPLETION---POW = 100%
Layer 1

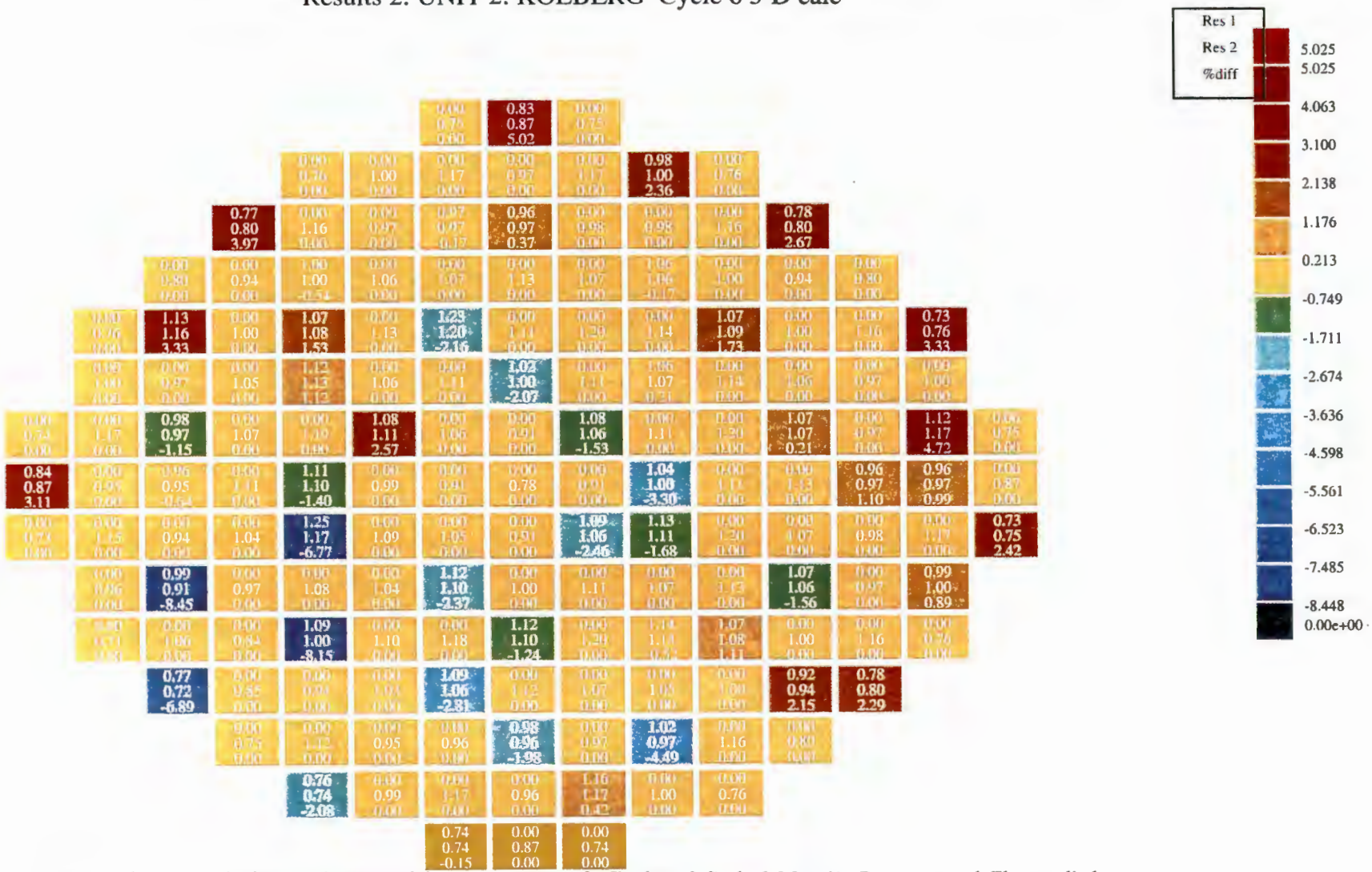

Differences between calculated and measured detector responses for Koeberg 2 Cycle 6 Map 61 : Reconstructed Flux applied

Detector Response - Reconstructed Flux

Colour: %diff